Since January 2020 Elsevier has created a COVID-19 resource centre with free information in English and Mandarin on the novel coronavirus COVID-19. The COVID-19 resource centre is hosted on Elsevier Connect, the company's public news and information website.

Cell Reports

Article

Recruitment of highly cytotoxic CD8+ T cell receptors in mild SARS-CoV-2 infection

Graphical abstract

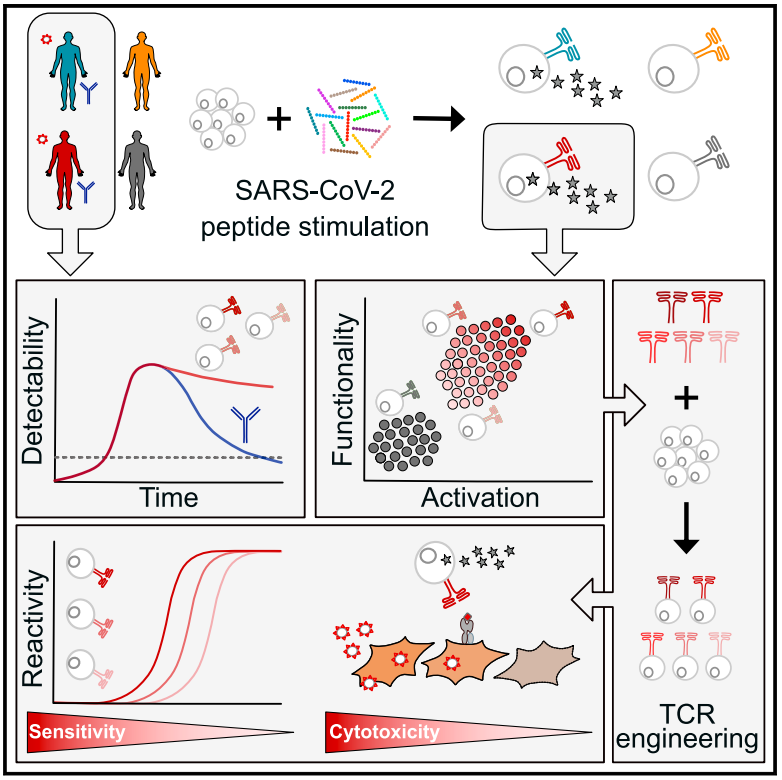

Highlights

- SARS-CoV-2-specific CD8+ T cells are detectable up to 12 months after infection
- scRNA sequencing reveals polyclonal CD8+ T cells with variable functionalities
- High-avidity CD8+ T cells engineered with SARS-CoV-2-specific TCRs are cytotoxic
- Single cell signature for highly functional SARS-CoV-2-specific CD8+ T cells

Authors

Karolin I. Wagner, Laura M. Mateyka, Sebastian Jarosch, ..., Markus Gerhard, Elvira D'Ippolito, Dirk H. Busch

Correspondence

elvira.dippolito@tum.de (E.D.), dirk.busch@tum.de (D.H.B.)

In brief

Wagner et al. detect CD8+ T cell responses to diverse immunodominant SARS-CoV-2-specific epitopes. scRNA sequencing of epitope-responsive CD8+ T cells reveals a polyclonal T cell receptor repertoire. State-of-the-art TCR re-expression confirms a highly specific and functional T cell response in convalescent mild COVID-19.

Wagner et al., 2022, Cell Reports *38*, 110214
January 11, 2022
https://doi.org/10.1016/j.celrep.2021.110214

CellPress

Cell Reports

CellPress
OPEN ACCESS

Article

Recruitment of highly cytotoxic CD8+ T cell receptors in mild SARS-CoV-2 infection

Karolin I. Wagner,[1,14] Laura M. Mateyka,[1,14] Sebastian Jarosch,[1,14] Vincent Grass,[2] Simone Weber,[1] Kilian Schober,[1,3] Monika Hammel,[1] Teresa Burrell,[1] Behnam Kalali,[1] Holger Poppert,[4,5] Henriette Beyer,[4] Sophia Schambeck,[1,4] Stefan Holdenrieder,[6] Andrea Strötges-Achatz,[6] Verena Haselmann,[7] Michael Neumaier,[7] Johanna Erber,[8] Alina Priller,[9] Sarah Yazici,[9] Hedwig Roggendorf,[9] Marcus Odendahl,[10,11] Torsten Tonn,[10,11] Andrea Dick,[12] Klaus Witter,[12] Hrvoje Mijočević,[2] Ulrike Protzer,[2,13] Percy A. Knolle,[9,13] Andreas Pichlmair,[2,13] Claudia S. Crowell,[1,13] Markus Gerhard,[1,13] Elvira D'Ippolito,[1,15,*] and Dirk H. Busch[1,13,15,16,*]

[1]Institute for Medical Microbiology, Immunology and Hygiene, Technical University of Munich (TUM), 81675 Munich, Germany
[2]Institute of Virology, School of Medicine, Technical University of Munich (TUM), 81675 Munich, Germany
[3]Mikrobiologisches Institut – Klinische Mikrobiologie, Immunologie und Hygiene, Universitätsklinikum Erlangen, Friedrich-Alexander-Universität (FAU) Erlangen-Nürnberg, 91054 Erlangen, Germany
[4]Department of Neurology, Helios Klinikum München West, 81241 Munich, Germany
[5]Neurologische Klinik, University Hospital Rechts der Isar, Technical University of Munich (TUM), 81675 Munich, Germany
[6]Institute of Laboratory Medicine, Munich Biomarker Research Center, Deutsches Herzzentrum München, Technical University of Munich (TUM), 80636 Munich, Germany
[7]Department of Clinical Chemistry, University Medicine Mannheim, Medical Faculty Mannheim of the University of Heidelberg, 68167 Mannheim, Germany
[8]Department of Internal Medicine II, University Hospital rechts der Isar, Technical University of Munich, School of Medicine, Munich, Germany
[9]Institute of Molecular Immunology and Experimental Oncology, School of Medicine, Technical University of Munich (TUM), 81675 Munich, Germany
[10]Experimental Transfusion Medicine, Medical Faculty Carl Gustav Carus, TU Dresden, 01307 Dresden, Germany
[11]Institute for Transfusion Medicine Dresden, German Red Cross Blood Donation Service North-East, 01307 Dresden, Germany
[12]Laboratory of Immunogenetics and Molecular Diagnostics, Department of Transfusion Medicine, Cellular Therapeutics and Hemostaseology, LMU University Hospital, 81377 Munich, Germany
[13]German Center for Infection Research (DZIF), Partner Site Munich, Munich, Germany
[14]These authors contributed equally
[15]Senior author
[16]Lead contact
*Correspondence: elvira.dippolito@tum.de (E.D.), dirk.busch@tum.de (D.H.B.)
https://doi.org/10.1016/j.celrep.2021.110214

SUMMARY

T cell immunity is crucial for control of severe acute respiratory syndrome coronavirus 2 (SARS-CoV-2) infection and has been studied widely on a quantitative level. However, the quality of responses, in particular of CD8+ T cells, has only been investigated marginally so far. Here, we isolate T cell receptor (TCR) repertoires specific for immunodominant SARS-CoV-2 epitopes restricted to common human Leukocyte antigen (HLA) class I molecules in convalescent individuals. SARS-CoV-2-specific CD8+ T cells are detected up to 12 months after infection. TCR repertoires are diverse, with heterogeneous functional avidity and cytotoxicity toward virus-infected cells, as demonstrated for TCR-engineered T cells. High TCR functionality correlates with gene signatures that, remarkably, could be retrieved for each epitope:HLA combination analyzed. Overall, our data demonstrate that polyclonal and highly functional CD8+ TCRs—classic features of protective immunity—are recruited upon mild SARS-CoV-2 infection, providing tools to assess the quality of and potentially restore functional CD8+ T cell immunity.

INTRODUCTION

Severe acute respiratory syndrome coronavirus 2 (SARS-CoV-2) is a new betacoronavirus responsible for coronavirus disease 2019 (COVID-19), a pathological condition that can progress to severe pneumonia and a fatal outcome (Zhou et al., 2020; Zhu et al., 2020). The adaptive immune system plays a critical role in SARS-CoV-2 infection. In most cases, T and B cells react quickly and in a coordinated manner to the infection (Mathew et al., 2020; Rydyznski Moderbacher et al., 2020; Suthar et al., 2020) and develop a robust memory pool detectable months after exposure regardless of disease severity (Peng et al., 2020; Sekine et al., 2020; Sokal et al., 2021). In line with this, individuals who recover from COVID-19 experience low reinfection rates, in particular for symptomatic infection (Deng et al., 2020; Hall et al., 2021; Hansen et al., 2021). In contrast, severe clinical manifestations occur in

the less frequent scenario where immune responses are suboptimal, i.e., in elderly individuals in whom antigen presentation is less efficient and the pool of naive T cells is scarce (Bacher et al., 2020; Rydyznski Moderbacher et al., 2020). Despite the increasing understanding of SARS-CoV-2 immunity, a clear correlate of protection is still missing. This is of paramount importance because it would allow identification of individuals with minimal risk of reinfection as well as the minority of individuals with a high risk of developing severe symptoms because of a lack of adequate immunity. In addition, it would provide relevant platforms or tools for validation of candidate vaccines, including immunity toward virus variants.

Antibody titers have been used extensively to describe SARS-CoV-2 adaptive immunity because their detection is suitable for high-throughput testing and intrinsically mirrors adequate recruitment of $CD4^+$ T cells. However, the role of antibodies in protective immunity is still controversial. Seropositive convalescent individuals show a lower risk of reinfection (Addetia et al., 2020; Hall et al., 2021; Lumley et al., 2021), but neither total nor neutralizing antibody titers protect from severe symptoms during primary infection (Rydyznski Moderbacher et al., 2020; Tan et al., 2021). In addition, the resolution of SARS-CoV-2 infection in individuals unable to produce antibodies (Soresina et al., 2020) further indicates that other immune compartments are rather essential for protective immunity.

Early induction of SARS-CoV-2-specific T cells has been shown to be associated with milder disease and less prolonged virus shedding (Rydyznski Moderbacher et al., 2020; Tan et al., 2021), and, remarkably, depletion of $CD8^+$ T cells abrogates protection against re-challenge in pre-clinical models (McMahan et al., 2021). This evidence strongly supports a key role of T cells in control and resolution of SARS-CoV-2 infection. This should hold true in particular for $CD8^+$ T cells because of their unique contribution to protection from intracellular pathogens (Huster et al., 2006) by direct killing of target cells. Of similar importance, T cells persist longer than waning antibodies (Peng et al., 2020; Sherina et al., 2021) and, thus, are more informative regarding long-term maintenance of functional SARS-CoV-2 immunity.

SARS-CoV-2-specific T cell immunity has been widely characterized quantitatively (Bacher et al., 2020; Peng et al., 2020; Quadeer et al., 2021; Sekine et al., 2020; Tarke et al., 2021). However, little is known about their quality and, therefore, determinants of protection. This lack of knowledge in the COVID-19 field mainly derives from broad use of single-dose peptide mixes (15-mers) for T cell analyses, which are often preferred because they can be designed easily to cover entire open reading frames (ORFs). Their use is highly valuable to gain information about the magnitude and breadth of SARS-CoV-2 T cell responses in a remarkably short time (Peng et al., 2020; Tarke et al., 2021) but at the expense of precision, i.e., the specificity and quality of single-epitope responses. Indeed, the epitopes responsible for the observed T cell reactivity are often unknown, and peptide mixes are usually used at a single high concentration, which hinders discrimination of high (protective) and low (suboptimal) functional T cells. This information has become extremely relevant because (1) a high frequency of cross-reactivity with common cold CoVs has been reported, although mainly for $CD4^+$ T cells (Le Bert et al., 2020; Braun et al., 2020; Grifoni et al., 2020; Mateus et al., 2020; Schulien et al., 2020), and (2) suboptimal but high-frequency T cell responses have been observed in individuals with severe COVID-19 because of recruitment of low functional cross-reactive memory T cells rather than highly specific naive T cells (Bacher et al., 2020). Finally, $CD8^+$ T cell responses are still under-represented and therefore less investigated because 15-mer peptides primarily stimulate $CD4^+$ T cells (Mateus et al., 2020). This evidence underlines how the detection and magnitude of T cell responses are not always equivalent to functionality.

Thus, we decided to investigate in depth the quality of SARS-CoV-2-specific $CD8^+$ T cells through analyses of their T cell receptor (TCR) repertoire. A TCR is the fingerprint of a T cell and determines its specificity, functionality, and fate. Furthermore, preclinical studies have shown that highly functional TCRs drive establishment of protective immunity in infectious diseases because they dominate primary infections (Zehn et al., 2009) and react faster to recall infections (Busch and Pamer, 1999). By analyzing the SARS-CoV-2 epitope-specific TCR repertoire in convalescent individuals who experienced mild symptoms and for whom, therefore, protective immunity should have established, we show that highly functional and polyclonal TCRs are recruited in $CD8^+$ T cell responses against SARS-CoV-2 during non-severe disease.

RESULTS

Detection of SARS-CoV-2-specific $CD8^+$ T cells through 9-mer peptide pool stimulation

To study SARS-CoV-2-specific $CD8^+$ T cell responses, we designed a pool of SARS-CoV-2 peptides (9-mer) predicted to be immunogenic for the most common human leukocyte antigen (HLA) class I molecules (HLA-A*01:01, A*02:01, A*03:01, A*11:01, A*24:02, B*07:02, B*08:01, and B*35:01). This HLA combination covers 73% of the European Caucasian population, 78% of Australia, 76% of Central and South America, 69% of North America, and 75% of Northeast Asia but only 53% of North Africa, 61% of South Asia, and 54% of Western Asia (cumulative HLA allele frequency, http://www.allelefrequencies.net; similar to Effenberger et al., 2019). We finally selected 40 candidates, among which nine showed 100% homology with SARS-CoV (Table S1). No homology was found with published epitopes (Immune Epitope Database, IEDB) from common cold CoVs (CCCoVs; 229E, NL63, HKU1, and OC43; degree of homology higher than 70%), and no hits with less than a four-amino-acid exchange were found in the global CCCoV genome (Table S2). Considering the strict rules that govern epitope binding to HLA class I molecules, this degree of homology strongly speaks against possible cross-reactivity between SARS-CoV-2 and CCCoV epitopes.

SARS-CoV-2 T cell responses contract and become barely detectable *ex vivo* within a few weeks after infection (Wang et al., 2021). Our cohort of convalescent individuals (PCR^+ with a mild course of disease and no need for hospitalization, referred to as mild COVID-19 hereafter) comprised blood sampled at least 30–50 days after infection. Therefore, we tested the sensitivity of *ex vivo* responses to a commercially available peptide

mix of the Spike (S) protein (Peptivator S, 15-mer mix), and, as expected, we detected low-frequency but reliable T cell responses in most mild COVID-19, mainly in $CD8^-$ T cells (Figures S1A and S1B). Stimulation with our 9-mer pool, however, indicated detectable T cell responses in only a few individuals. Size of frequency and robustness of detection were, in addition, suboptimal (Figures S1A and S1B), primarily because of the small size of our pool (4-fold lower number of peptides than the Peptivator S pool). Thus, to detect such low-frequency SARS-CoV-2-reactive $CD8^+$ T cell populations, we adapted an expansion protocol where T cells are stimulated with autologous pulsed peripheral blood mononuclear cells (PBMCs) and *in vitro* expanded prior re-challenge and T cell functional analyses (Oh et al., 2011) (Figure 1A). We successfully observed SARS-CoV-2 T cell responses after expansion in a set of subjects with mild COVID-19; furthermore, as expected by the design of the 9-mer peptide pool, primarily $CD8^+$ but not $CD8^-$ T cells responded to the stimulation (Figures S1C and S1D).

SARS-CoV-2-specific $CD8^+$ T cell responses persist long term in convalescent and asymptomatic seropositive individuals

We next studied such T cell responses across four distinct cohorts: 53 individuals with mild COVID-19, 28 asymptomatic seropositive individuals, 37 asymptomatic individuals who continuously tested seronegative for SARS-CoV-2 immunoglobulin G (IgG) antibodies throughout the observation period, and 28 unexposed individuals from whom blood was collected before the outbreak (Table S3).

Individuals with mild COVID-19 and asymptomatic seropositive individuals showed strong, although variable, $CD8^+$ T cell response rates (81% and 78%, respectively). In contrast, responses were observed in a small proportion of asymptomatic seronegative and unexposed individuals, the latter also particularly weak (Figures 1B and 1C). T cell responses can develop in the absence of antibody production (Sekine et al., 2020), supporting our findings in asymptomatic seronegative individuals. Reactivity in pre-pandemic individuals has been explained as cross-reactive T cells (Grifoni et al., 2020; Nelde et al., 2020; Schulien et al., 2020) or associated with an exceptionally high naive precursor frequency (Nguyen et al., 2021). As before, $CD8^+$ T cells dominated the overall T cell responses after *in vitro* peptide expansion (Figures 1C and S1E). Importantly, for the majority of HLA class I molecules included in the SARS-CoV-2 epitope prediction, the coverage among the four cohorts was at comparable levels (Figure S2), excluding a bias in T cell responses because of a different HLA representation.

Except for pre-pandemic donors, blood was collected over several months, allowing us to investigate the longevity of SARS-CoV-2 $CD8^+$ T cell immunity. We first looked at $CD8^+$ T cell responses and antibody titers at early time points after diagnosis (PCR test) for mild COVID-19 and after enrollment in the study for asymptomatic seropositive cohorts. We observed concomitantly detectable levels of SARS-CoV-2-specific IgG and $CD8^+$ T cells in the majority of individuals (Figure 1D). This is in line with previous reports describing coordinated responses of the humoral and T cell arms in individuals who resolved the infection without severe symptoms (Rydyznski Moderbacher et al., 2020). Despite the fact that antibody titers waned rapidly over time (Figure 1E), SARS-CoV-2-specific $CD8^+$ T cells remained relatively stable (Figure 1F), similar to other reports (Peng et al., 2020; Sherina et al., 2021), and, remarkably, were detected up to 12 months after infection (Figure 1G).

Overall, we could show that the designed 9-mer pool can be used to detect SARS-CoV-2 $CD8^+$ T cell responses regardless of symptom severity and that long-lasting $CD8^+$ T cell immunity establishes upon primary infection.

Identification of immunodominant SARS-CoV-2 $CD8^+$ T cell epitopes

Before investigating the functionality of SARS-CoV-2-specific TCR repertoires, we searched our 9-mer pool for immunodominant epitopes to study $CD8^+$ T cell responses specific for single epitopes that might have high relevance to SARS-CoV-2 infection.

To do so, we applied a two-step deconvolution process where expanded PBMCs were first re-stimulated with one of four distinct subpools, each composed of 8–12 peptides, and then analyzed for the individual epitopes of the reactive subpools. We performed this deconvolution on mild COVID-19 responders for whom HLA class I genotyping was available. In total, we found 19 immunogenic peptides, despite a certain variability in the magnitude of responses and the number of responders (Figures 2A and S3). Except for ORF1_LTN and ORF1_HSI, immunogenicity of the remaining epitopes has also been reported in other studies (Le Bert et al., 2020; Ferretti et al., 2020; Habel et al., 2020; Nelde et al., 2020; Peng et al., 2020; Schulien et al., 2020; Table S1). Interestingly, we often observed $CD8^+$ T cell responses against multiple epitopes deriving from the same SARS-CoV-2 ORF (e.g., donors 11 and 12) as well as from different ORFs in individual donors (e.g., donors 14 and 24) (Figure 2A), indicating that broad and polyclonal $CD8^+$ T cell response are elicited upon infection.

We also assessed the specificity of the identified immunogenic epitopes to SARS-CoV-2 through evaluation of single-peptide responses in pre-pandemic responders. Only in four of them we did confirm $CD8^+$ T cell reactivity. In addition, we observed responses to only one epitope per donor and at low magnitude (Figure 2A), overall highlighting how less consistent these responses are compared with mild COVID-19. All four epitopes stimulating $CD8^+$ T cells in pre-pandemic individuals were also found to be immunogenic in mild COVID-19. Despite similar frequencies in unexposed individuals (except for B35/ORF1_VPF), the ORF1_DTD and ORF3_FTS epitopes showed remarkably high immunodominance in mild COVID-19 (Figure 2B), which could be explained by an unusually high naive precursor frequency (Nguyen et al., 2021) or pre-existing immunity (Niessl et al., 2021). In contrast, similar percentages of responders were found in individuals with mild COVID-19 and unexposed individuals for the A2/N_LLL and B35/OFR1_VPF epitopes, which would better support the hypothesis of cross-reactive epitopes with limited relevance in SARS-CoV-2 infection. Additional analyses would be necessary to comprehensively decipher the source of pre-pandemic responses.

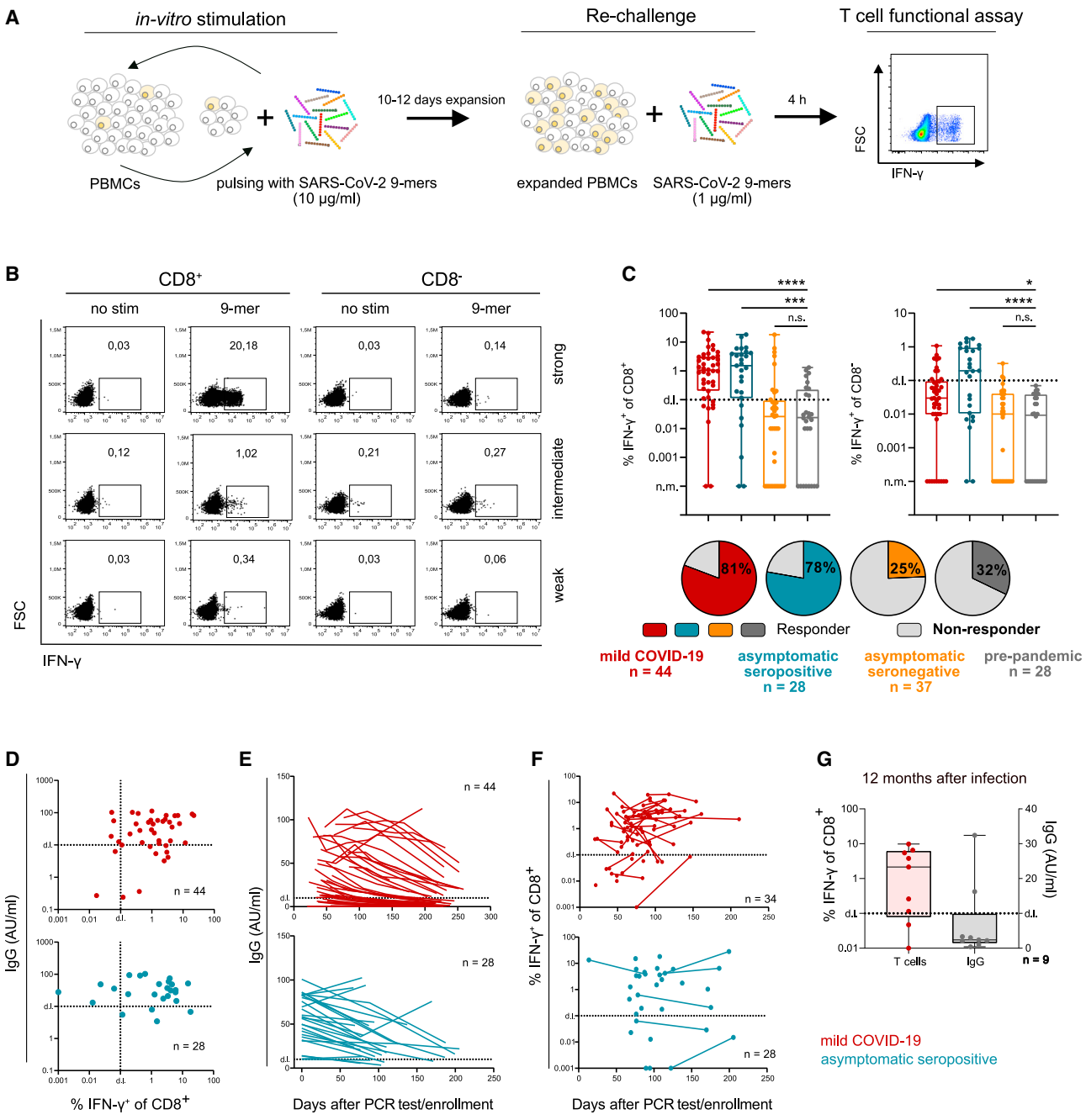

Figure 1. Long-term persistence of SARS-CoV-2-specific CD8$^+$ T cells in individuals with mild COVID-19 and asymptomatic seropositive individuals

(A) Schematic overview of the *in vitro* expansion protocol for detection of CD8$^+$ T cell responses.

(B and C) 5 × 10^6 PBMCs were treated as described in (A). Depicted are representative raw data (B) and quantification (C) of IFN-γ-releasing T cells upon 9-mer peptide pool re-stimulation after expansion. Responders were identified respective to the non-stimulated negative control (detection limit set to 0.1% IFN-γ$^+$ CD8$^+$/CD8$^-$ T cells after background subtraction). Data are depicted in a box and whiskers plot - min to max, all points shown. The box extends from the 25th to 75th percentiles, and the middle line indicates the median value. Statistical analyses were performed via one-way ANOVA with Kruskal-Wallis test (*p < 0.05, ***p < 0.001, ****p <0.0001).

(D–G) SARS-CoV-2-specific IgG and CD8$^+$ T cells were measured for individuals with mild COVID-19 (red) and asymptomatic seropositive (blue) individuals at their first follow-up visit (62.4 ± 20.4 days after PCR-confirmed infection and 102.6 ± 24.5 days after study enrollment, respectively) (D), throughout the observation period (connected lines indicate different time points for the same individual) (E and F), and 1 year after PCR-confirmed infection (G). In (G), data are depicted in a box and whiskers plot - min to max, all points shown. The box extends from the 25th to 75th percentiles, and the middle line indicates the median value. For flow cytometry analyses, reactive cells were pre-gated on CD3$^+$ living lymphocytes.

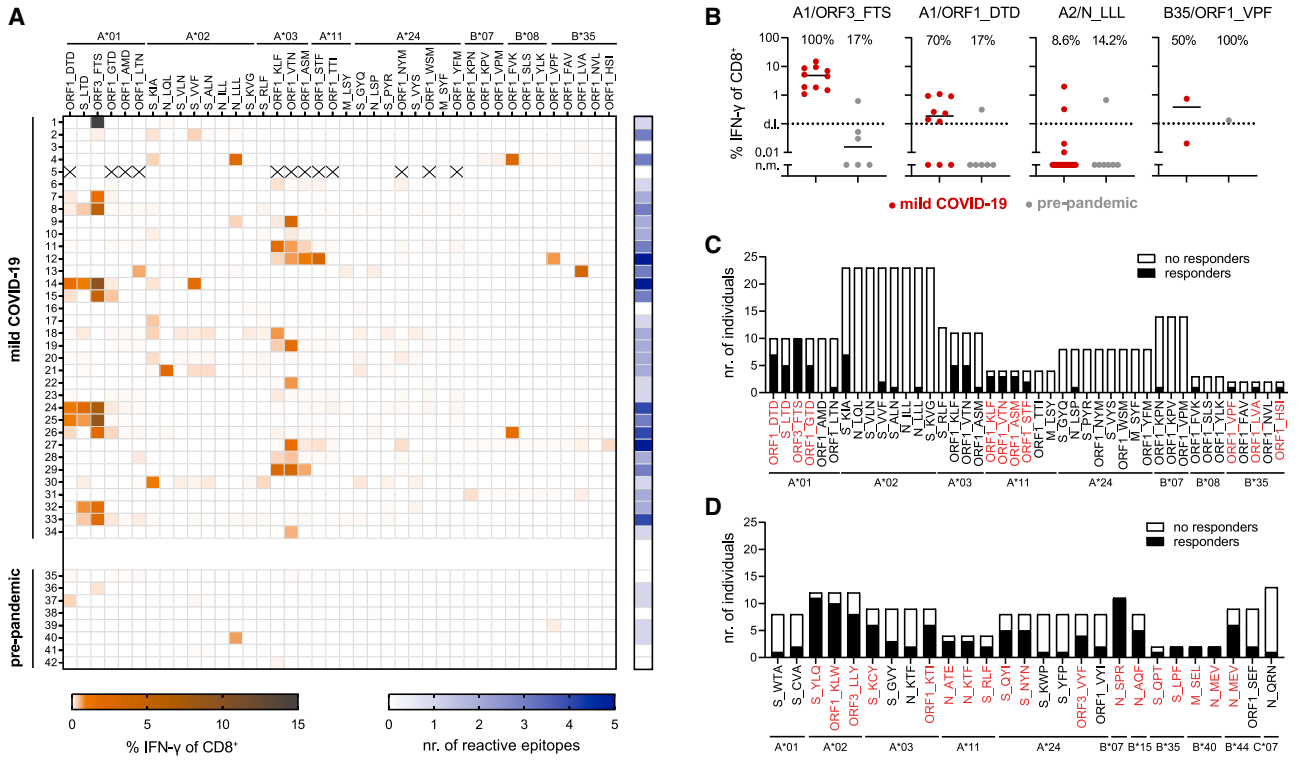

Figure 2. Identification of immunodominant SARS-CoV-2-specific CD8$^+$ T cell epitopes

(A) Heatmap showing the percentage of CD8$^+$ T cells producing IFN-γ in response to individual peptide stimulation (orange-black gradient scale) and the number of reactive epitopes (blue-white gradient scale) in mild COVID-19 (donors 1–34, n = 34) and pre-pandemic (donors 35–42, n = 8) individuals. Crosses indicate data not available.

(B) Comparison of CD8$^+$ T cell responses to specific epitopes in mild COVID-19 and pre-pandemic individuals. Percentages indicate immunodominance.

(C and D) Immunodominance of individual SARS-CoV-2 epitopes in individuals with mild COVID-19 for peptides of the in-house 9-mer peptide pool (C) and subsequent peptide selection to increase HLA coverage (D). Peptides inducing a more than 50% response rate in HLA-matched donors are marked in red. For flow cytometry analyses, reactive cells were pre-gated on CD3$^+$ living lymphocytes.

Next, to understand the relevance of the identified immunogenic epitopes in SARS-CoV-2 T cell immunity, we quantified their immunodominance. Among the 19 immunogenic SARS-CoV-2 epitopes, 11 showed an immunodominance of at least 50% (Figure 2C). By combining the responses of individual epitopes restricted to the same HLA class I molecule, we achieved a response rate of 100% for HLA-A*01:01, HLA-A*11:01, and B*35:02 and 63% for HLA-A*03:01 but only 40% for HLA-A*02:01, 33% for HLA-B*08:01, and less than 15% or no responses for the remaining HLAs (Figure S4A). To increase HLA coverage, we tested a second pool of SARS-CoV-2-derived 9-mers composed of a mixture of newly predicted and published epitopes (Table S1). We confirmed 27 additional immunogenic epitopes, of which 17 displayed an immunodominance higher than 50% (Figures 2D and S4B). Furthermore, we sharply increased the response rate for HLA-A*02:01 (70%), A*24:02 (78%), and B*07:02 (100%) and gained coverage for HLA-B*40:01 (100%) and B*44:03 (60%) (Figure S4A).

Altogether, we identified a pool of immunodominant SARS-CoV-2 epitopes that could specifically identify individuals who had been exposed to the virus. Indeed, despite sporadic responses in non-infected individuals, the pattern of multiple-epitope responses makes convalescent individuals uniquely distinguishable.

Isolation of SARS-CoV-2-specific HLA class I-restricted TCRs

Previous analyses have revealed several promising CD8$^+$ T cell epitopes with high immunodominance and specificity to SARS-CoV-2 but without providing any information regarding the quality of the detected T cell responses. To fill this knowledge gap, we identified and functionally characterized SARS-CoV-2 epitope-specific TCR repertoires.

We first focused on two immunodominant SARS-CoV-2 epitopes restricted to frequent HLA class I molecules (A1/ORF3a_FTS and A3/ORF1_VTN). PBMCs from individuals with HLA-matched, mild COVID-19 were expanded on the 9-mer pool and re-challenged with individual epitopes prior to flow cytometry cell sorting, eventually followed by single-cell RNA sequencing (scRNA-seq). In addition to CD8$^+$interferon γ (IFN-γ)$^+$ T cells, which should be enriched in freshly re-activated T cells specific for the investigated epitopes, we also sorted CD8$^+$IFN-γ$^-$ T cells where TCRs specific for other immunogenic epitopes of the 9-mer pool or completely unrelated pathogens could be found (Figures 3A and S5A). Moreover, sorting of

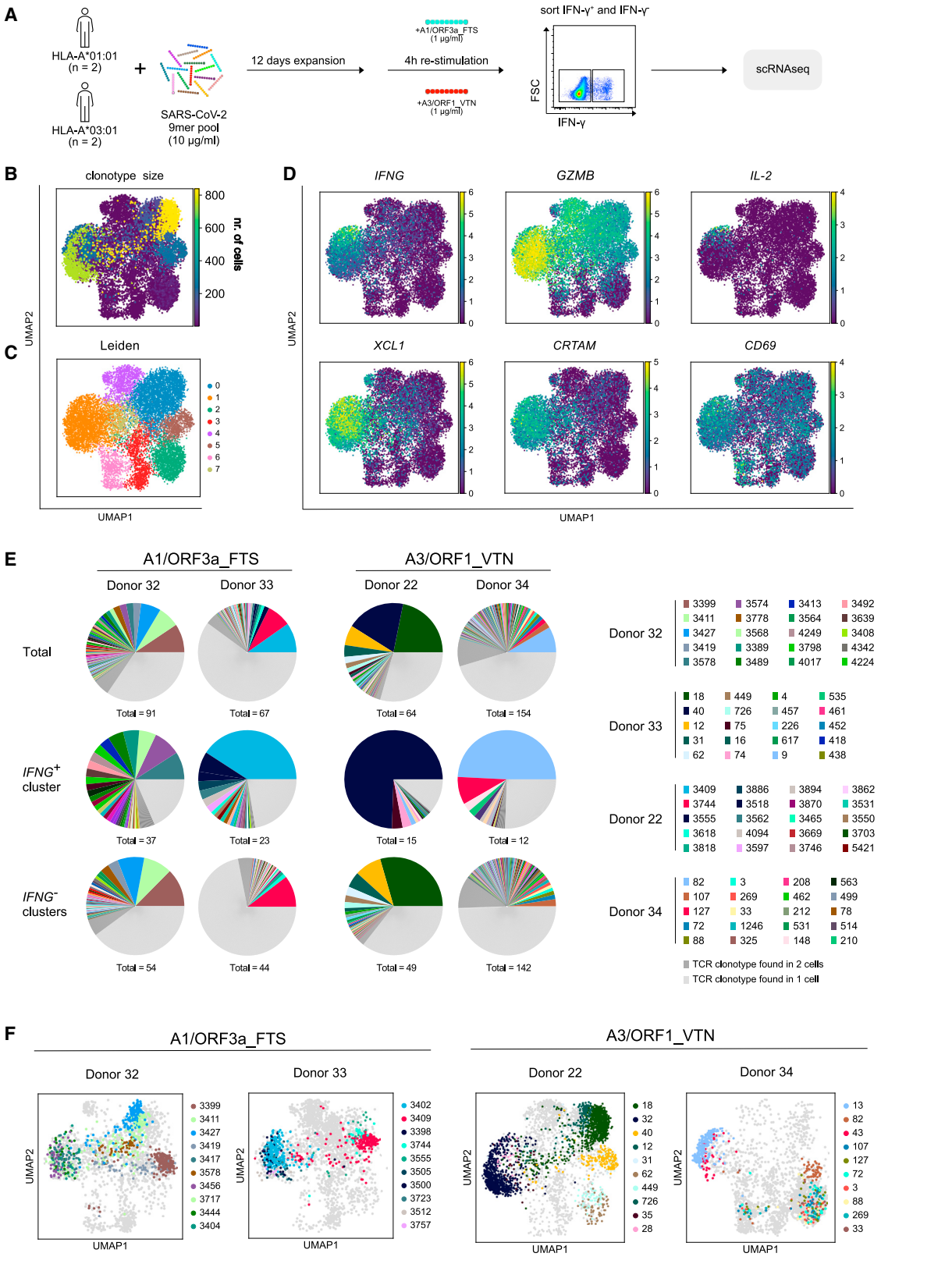

(legend on next page)

IFN-γ-secreting cells quantitatively caught most of the TCR repertoire, which is otherwise potentially limited by the relative low frequency of IFN-γ^+CD8$^+$ T cells; IFN-γ^- sorted T cells also served as control group for comparative transcriptomics analyses. In this way, on one hand, most of the information about the SARS-CoV-2-specific TCR repertoire of a donor would be retrieved without losing focus on the epitopes of highest interest. On the other hand, the potential of gene signatures to infer TCR specificity and functionality may be explored.

Analysis of clonotypic expansion and Leiden clustering revealed that the most expanded TCR clonotypes were present in clusters 0, 1, and 5 (Figures 3B and 3C), indicating that these three clusters may contain activated and expanded SARS-CoV-2-specific T cells. Particularly cluster 1 contained cells with high and, for some markers, unique expression of effector molecules (*IFNG*, *GZMB*, and *IL-2*) and activation markers (*XCL1*, *CD69*, and *CRTAM*) (Figure 3D). The XCL1 chemokine is produced by activated T cells during infection and inflammatory responses and interacts with the XCR1 receptor on dendritic cells, promoting dendritic cell-mediated cytotoxic immune responses (Brewitz et al., 2017). *CRTAM* is expressed on activated T cells (Patiño-Lopez et al., 2006; Rojas-Marquez et al., 2015) and coordinates cell polarity during activation, which has been shown to be crucial for production of effector cytokines (Yeh et al., 2008). Together with up-regulation of the *IFNG*, *GZMB*, *IL-2*, and *CD69* genes, this signature of recent activation may suggest an enrichment of T cells specific for the A1/ORF3a_FTS and A3/ORF1_VTN epitopes in cluster 1. Considering the basal levels of GzmB in memory T cells (Grossman et al., 2004; Lin et al., 2014), the only expression of *GZMB*, but not of *IFNG*, *XCL1*, and *IL-2*, in clusters 0 and 5 suggested instead the presence of late activated T cells, presumably reactive toward SARS-CoV-2 epitopes other than A1/ORF3a_FTS and A3/ORF1_VTN.

Pooled samples were deconvoluted according to single-nucleotide polymorphisms (Xu et al., 2019) and assigned to an individual donor by sex and HLA class I genotype (Figures S5B–S5E). All donors showed a polyclonal TCR repertoire (Figure 3E) with the dominating clonotypes distributed among clusters 0, 1, and 5 (Figure 3F). The TCR repertoire for cluster 1 (*IFNG*$^+$ cluster) was highly diverse, in particular in the case of ORF3a_FTS, and showed a higher fraction of clonally expanded TCRs (Figure 3E).

We found that SARS-CoV-2-specific TCR repertoires are highly polyclonal, with some clonotypes showing a prominent signature of recent activation, presumably reflecting fresh re-stimulation.

SARS-CoV-2-specific TCR repertoires contain highly functional TCRs

To investigate the quality of the identified SARS-CoV-2-specific TCR repertoires, we next re-expressed candidate TCRs for functional characterization by CRISPR-Cas9-mediated orthotopic TCR replacement (OTR). Here, complete replacement of the endogenous TCR is achieved by transgenic TCR knockin (KI) into the endogenous TCR α locus and concomitant TCR β locus knockout (Schober et al., 2019). We selected TCRs from cluster 1 and clusters 0 and 5 among the top 10 expanded clonotypes (Figures 3F, S5E, and S5F; Table S4). Thus, potential associations between TCR specificity/functionality and the observed activation signature could be analyzed.

We first validated the specificity of our transgenic TCRs via epitope-HLA multimer staining because false epitope-specific TCRs may be retrieved. All TCRs selected from cluster 1 (*IFNG*$^+$ cluster) showed strong staining toward relevant multimers (ORF1_VTN and ORF3a_FTS), except for A3/TCR 32, which stained weaker; no reactivity was observed against irrelevant multimers (HLA-A*03:01 or HLA-A*01:01 multimers loaded with a different epitope), confirming specific epitope recognition (Figures 4A and 4B). Instead, none of the TCRs selected from clusters 0 and 5 (*IFNG*$^-$ cluster) reacted to the relevant multimers, but A3/TCR 40 showed specificity for ORF1_KLF (Figures 4A and 4B). To decipher the specificity of the remaining *IFNG*$^-$ cluster-derived TCRs, we stimulated TCR-engineered T cells with autologous PBMCs pulsed with SARS-CoV-2 9-mer, cytomegalovirus (CMV), and Epstein-Barr (EBV) peptide pools because of the high prevalence of CMV and EVB infection in the human population and the induced big T cell responses (Callan et al., 1996; Sylwester et al., 2005). Cytokine release was observed only for A1/TCR 3399 (Figure S6). Altogether, HLA multimer staining confirmed that cluster 1 was enriched in freshly re-stimulated TCRs and that signatures of recent activation are indicative of TCR specificity to recent epitope re-challenge.

TCRs with clear specificity for SARS-CoV-2 epitopes were characterized further. All TCR-engineered T cells responded to the cognate peptide stimulus in a dose-dependent manner, and the majority showed sensitivity to very low peptide concentrations, as indicated by the IFN-γ EC_{50} values. A3/TCR 13, A3/TCR 28, A1/TCR 3398, and A1/TCR 3456 showed particularly high functionality with half-maximum cytokine release at peptide stimulation above 10^{-7} M, whereas A3/TCR 43 and A3/TCR 32 showed intermediate and low functionality, respectively (Figures 4C and 4D).

To test for cytotoxicity, we generated a target cell line susceptible to SARS-CoV-2 infection. Briefly, the A549 human lung cancer cell line was engineered to express the ACE2 protein, red fluorescent protein, and HLA-A*01:01 or HLA-A*03:01 molecules, which allowed viral infection, live-cell imaging acquisition, and appropriate epitope presentation, respectively. A genetically modified GFP-expressing SARS-CoV-2 virus was used for

Figure 3. Isolation of SARS-CoV-2-specific TCRs

(A) Schematic of the strategy for isolating SARS-CoV-2-specific TCRs. For each donor, 2,500 CD8$^+$IFN-γ^+ and 10,000 CD8$^+$IFN-γ^- T cells were sorted sequentially in the same well. Donors with same HLA background were further pooled prior processing for scRNA-seq.

(B) Uniform Manifold Approximation and Projection (UMAP) neighborhood embedding showing distribution of TCR clonotypes and corresponding sizes.

(C) Depiction of Leiden clustering (resolution = 0.5) according to the neighborhood embedding.

(D) UMAP neighborhood embedding showing distribution of T cell function and activation markers.

(E) Pie chart showing the percentage of each TCR clonotype of the total repertoire (top), Leiden cluster 1 (center), and all Leiden clusters except for 1 (bottom).

(F) Distribution of the top 10 TCR clonotypes within the neighborhood embedding for each donor.

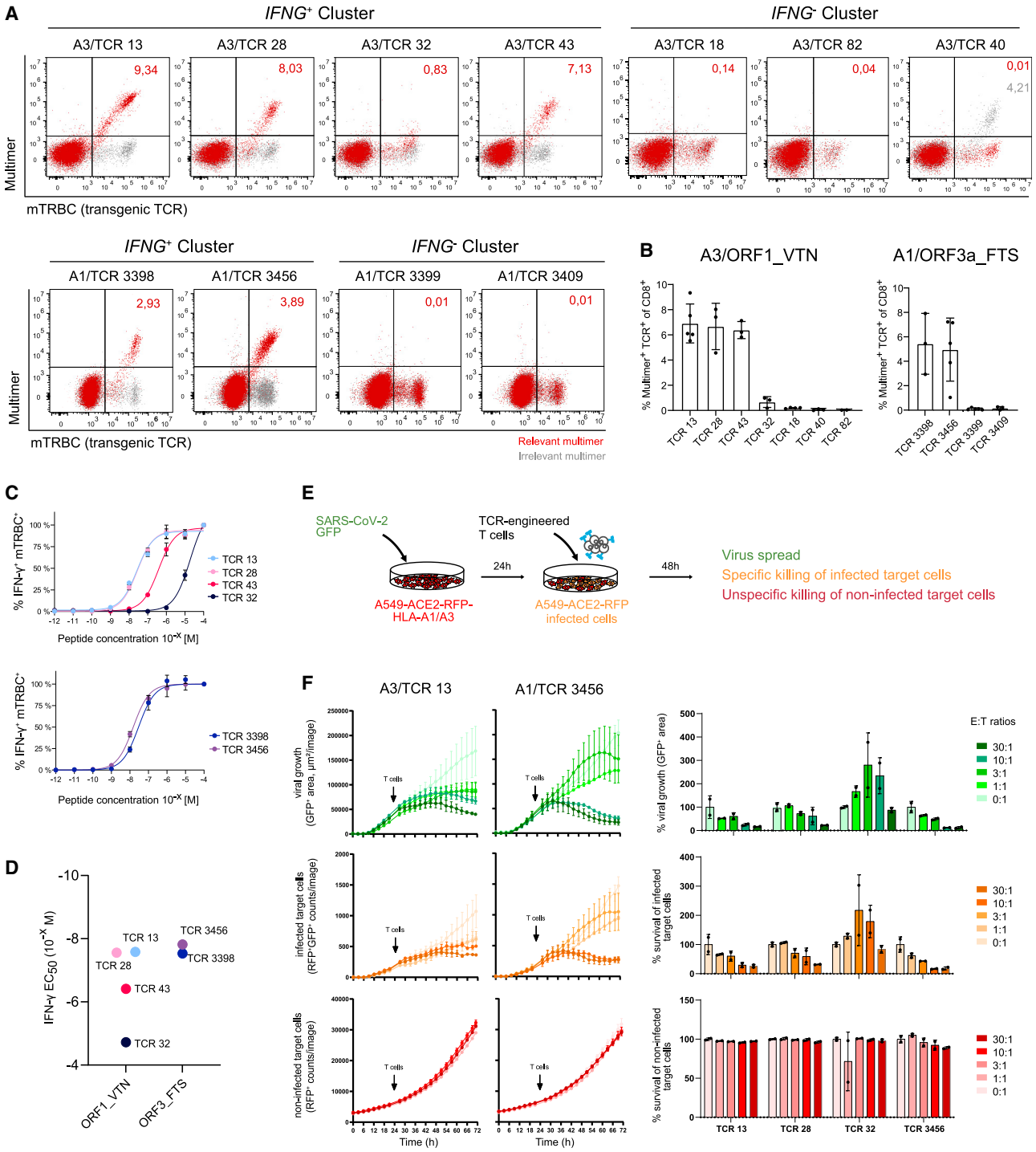

Figure 4. Identification of highly functional and cytotoxic SARS-CoV-2-specific TCRs

PBMCs from healthy donors were engineered to express a transgenic TCR, which contained a murine constant region, via CRISPR-Cas9-mediated orthotopic replacement.

(A and B) TCR-engineered T cells were stained with peptide-HLA multimers loaded with A1/ORF3a_FTS or A3/ORF1_VTN epitopes (relevant multimer) in addition to anti-CD8 and anti-murine T cell receptor beta chain (mTRBC) antibodies. As a control, multimers loaded with A1/pp50$_{245–253}$ or A3/OFR1_KLF (irrelevant multimers) were used. Shown are (A) representative examples and (B) quantification of multimer$^+$ TCR-KI$^+$ of CD8$^+$ cells of at least two independent TCR editing events in two different donors. In (B), data are shown as mean ± SD. Cells were pre-gated on CD8$^+$ living lymphocytes.

(C) Intracellular IFN-γ staining of T cells engineered with SARS-CoV-2-specific TCRs. Shown are representative plots of two independent experiments with two technical replicates.

(legend continued on next page)

infection. After viral infection, addition of TCR-engineered T cells successfully blocked viral spread (GFP signal) and induced killing of infected target cells (RFP^+GFP^+) with minimal off-target toxicity on non-infected cells (RFP^+) (Figures 4E and 4F). Only A3/TCR 32 again showed extremely low functionality, in line with the low levels of cytokine release upon epitope re-stimulation.

In summary, we showed that the TCR repertoire specific for the SARS-CoV-2 ORF1_VTN and ORF3a_FTS epitopes contains highly functional and cytotoxic TCRs. Furthermore, expression of genes related to recent activation is indicative of epitope specificity.

Functional SARS-CoV-2-specific TCRs are recruited in non-severe SARS-CoV-2 infection

The validated TCRs compose only a minor part of the total repertoire we isolated from ORF1_VTN- and ORF3a_FTS-specific T cells. Expression of *IFNG*, among other genes, was indicative of epitope specificity because it reflected reactivity after fresh re-stimulation prior to sorting and sequencing. Therefore, we searched our transcriptomic dataset for gene signatures that could associate with T cell functionality to also accurately predict functionality for non-validated TCRs.

Taking into consideration that TCRs were isolated from *in-vitro*-expanded $CD8^+$ T cells after fresh re-stimulation, we analyzed the predictive potential of an available gene signature related to $CD8^+$ T cell activation. The $CD8^+$ T cell activation score was enriched in cells expressing freshly re-stimulated TCRs, but it showed only a trend of correlation with T cell functionality (IFN-γ EC_{50}) among the reactive TCRs (Figure 5A). To improve the sensitivity of prediction, we defined two additional gene signatures more specific for our dataset and based on gene expression of cells expressing the TCRs we selected for re-expression and characterization; a "reactivity signature" composed of genes differentially expressed between epitope-reactive TCRs and non-reactive TCRs (Figure S7A), and a "functionality signature" comprising genes that best correlated with IFN-γ EC_{50} (Figures S7B and S7C). Epitope-reactive TCRs showed high scores for both signatures, and, remarkably, the functionality score accurately predicted T cell functionality. The percentage of $IFNG^+$ cells, but not the clonotype size, also clearly identified epitope-reactive TCRs but was not sufficient to resolve low (TCR 32) and highly functional TCRs (TCR 13 and TCR 28 among others) (Figure 5A). When applied to the entire set of identified TCR repertoires, high activation and functionality scores clearly separated and identified SARS-CoV-2-specific T cells responding to the recent re-stimulation, which were almost all belonging to the $IFNG^+$ cluster (Figure 5B). More importantly, within the reactive TCRs, clonotypes distributed among a range of signature scores. We found a relevant proportion of TCRs with scores similar to the high-avidity TCRs (3456, 3398, 28, and 13), except for donor 22, for whom a higher amount of low functional TCRs was observed. Intriguingly, low-avidity TCR 32 correspondingly showed intermediate positioning in the activation/proliferation score landscape (Figure 5B). Overall, our data indicate that a polyclonal population of highly functional TCRs is recruited in mild COVID-19 despite a variable proportion of intermediate- and low-avidity TCRs.

We finally expanded this TCR repertoire analysis to nine additional immunodominant SARS-CoV-2 epitopes restricted to five different HLA class I molecules in eight individuals with mild COVID-19. Each donor was stimulated with specific epitopes of interest, and expanded *in vitro* prior to re-stimulation and sorting of $CD8^+$IFN-γ^+ cells. Each sample was additionally labeled with a DNA-tagged antibody to make it distinguishable when pooled with other donors for scRNA-seq (Figure 6A). Despite sorting, transcriptomics data revealed heterogeneous expression of genes related to T cell function and activation, which resulted in different enrichment in the reactivity, functionality, and activation scores (Figure 6B). High reactivity scores were observed broadly, suggesting that the majority of the isolated repertoires should be specific to SARS-CoV-2. In addition, a fraction of those TCRs was also particularly enriched in the functionality score as well as in the activation score, indicating the presence of TCRs of presumably high functionality (Figure 6B). For a better evaluation, we correlated the reactivity and functionality scores for each clonotype of the newly identified repertoires, and we used the *in-vitro*-characterized TCRs as controls. We observed a bimodal distribution, with the functional transgenic TCRs (13, 28, 43, 3456, and 3398) occupying the $score^{high}$ cluster and the low-avidity (TCR 32)/non-specific TCRs (18, 40, 82, 3409, and 3399) showing low scores. All other clonotypes distributed within the reactivity/functionality landscape and a relevant number of clonotypes overlaid with highly functional transgenic TCRs (Figure 6C), further corroborating our initial observations.

As a final step, we wanted to understand the functional landscape of epitope-specific TCR repertoires. After deconvolution, most of the donors again showed a highly polyclonal TCR repertoire (Figure 6D). Remarkably, highly functional TCRs (defined by high gene signature scores) were predicted for all donors and analyzed SARS-CoV-2 epitopes (Figure 6E).

In conclusion, we could show that polyclonal $CD8^+$ T cell responses are elicited against immunodominant SARS-CoV-2 epitopes and that highly functional TCRs are recruited in mild COVID-19 despite some variability according to HLA-epitope combination.

DISCUSSION

The importance of $CD8^+$ T cells in respiratory virus infections is well recognized. $CD8^+$ T cells are recruited to the lungs within 8–10 days after infection (Flynn et al., 1998; Heidema et al., 2008; Lukens et al., 2006), contribute to viral clearance (Jozwik

(D) IFN-γ EC_{50} of SARS-CoV-2 TCR-engineered T cells shown in (C).
(E) Schematic of the T cell cytotoxicity assay. 24 h after infection, target cells were co-cultured with sorted TCR-engineered $CD8^+$ T cells at different effector-to-target (E:T) ratios for an additional 48 h. As a control, engineered T cells were also added to non-infected cells.
(F) Live tracking (left) and endpoint quantification (right) of viral spread (GFP^+), infected cells (GFP^+RFP^+) and non-infected cells (RFP^+). For endpoint analyses, infected cells were washed before signal acquisition. Data are shown as mean ± SD and are representative of one out of three independent experiments.

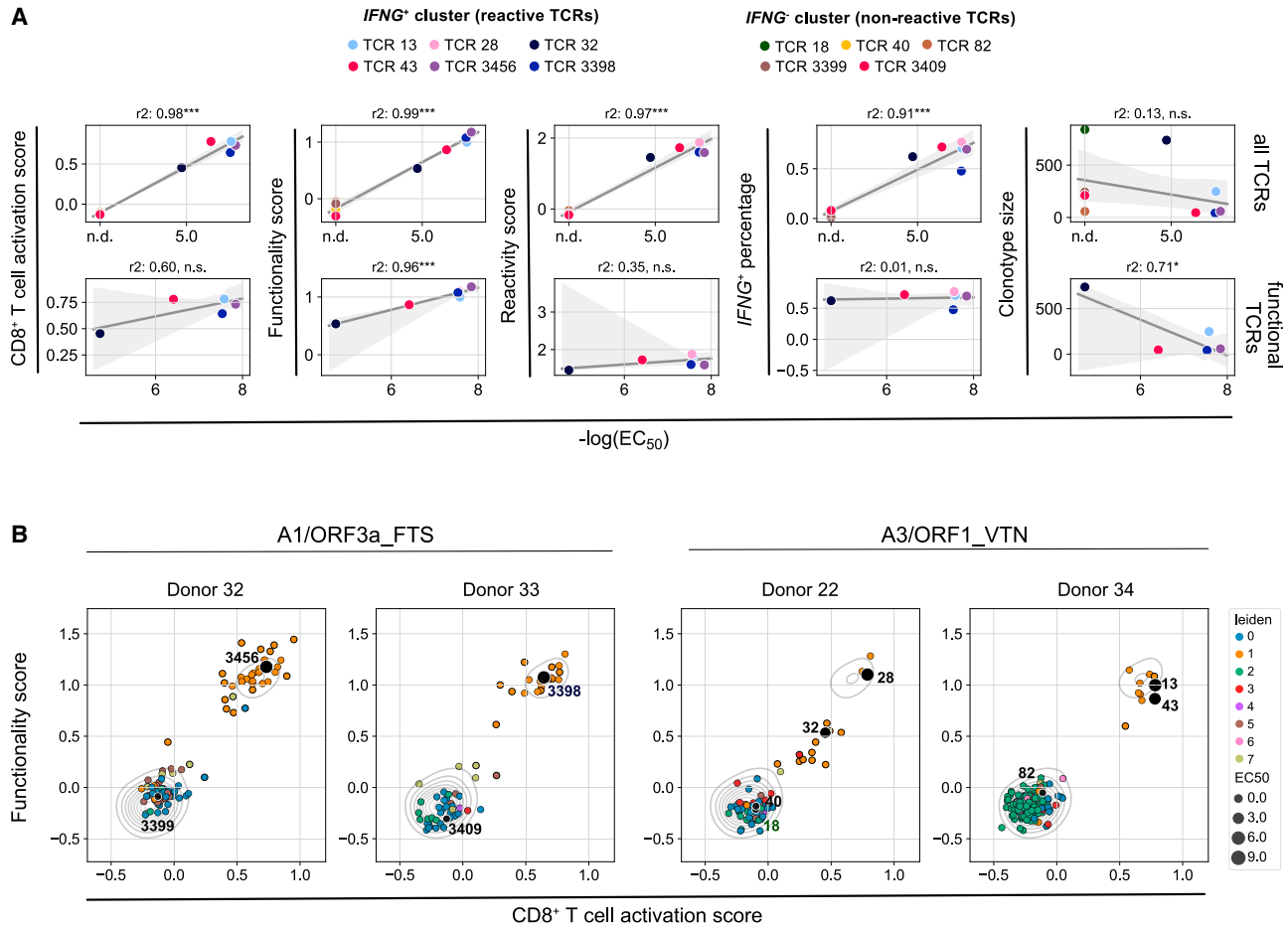

Figure 5. Highly functional TCRs correlate with a signature of recent activation

(A) Linear regression analysis between *in vitro* functionality (IFN-γ EC_{50}) and gene scores for all (top row) and functional (bottom row) TCRs. The gray area depicts the 95% confidence interval. *p < 0.05 and ***p < 0.001. Two-sided p values for a hypothesis test (null hypothesis; slope is zero) were calculated using a Wald test with t-distribution of the test statistic.

(B) TCR clonotype distribution according to $CD8^+$ T cell activation score and functionality score. The color code refers to the Leiden clusters, and the dot size of the re-expressed TCRs corresponds to the IFN-γ EC_{50} value. Contours show kernel density estimates (KDEs) of the pooled dataset including the four donors depicted in the individual plots.

et al., 2015; Lukacher et al., 1984; Yap et al., 1978), and generate a pool of memory cells that protect from re-infection (Heidema et al., 2008; Jozwik et al., 2015). In SARS-CoV infection, $CD8^+$ T cells provided substantial protection in preclinical studies (Channappanavar et al., 2014), and long-lasting memory SARS-CoV-specific $CD8^+$ T cells have been detected up to 17 years after infection in humans (Le Bert et al., 2020). T cell immunity against SARS-CoV-2 shares many of the abovementioned aspects. Early recruitment of T cells prevents severe disease (Tan et al., 2021) and is usually followed by establishment of a robust pool of functional memory T cells (Schulien et al., 2020; Sekine et al., 2020) detectable up to 6–10 months after infection (Dan et al., 2021; Jung et al., 2021; Sherina et al., 2021; Zuo et al., 2021). In addition to this existing body of evidence, we further showed that SARS-CoV-2-specific $CD8^+$ T cells are detectable up to 12 months after infections, pointing toward long-lasting immunity similar to SARS-CoV. Of course, continuous follow-up is necessary to strengthen the interpretation of even longer maintenance of $CD8^+$ T cell immunity.

However, whether and how $CD8^+$ T cells may mediate protective immunity in SARS-CoV-2 infection needs to be investigated in more detail. Despite encouraging preclinical data showing loss of protection following $CD8^+$ T cell depletion (McMahan et al., 2021), evidence of the protective role of $CD8^+$ T cells in humans is still scarce. SARS-CoV-2-reactive $CD8^+$ T cells have often been functionally characterized using *ex vivo* antigen stimulation-based assays (i.e., IFN-γ ELISpot assays, intracellular cytokine staining, and activation-induced markers), but use of a single peptide (or peptide mix) dose hinders discrimination of high and low functional T cells. T cell functionality is primarily encoded in its TCR. For this reason, as a first step toward a deeper understanding of the quality of $CD8^+$ T cell responses against this new virus, we investigated the functionality of SARS-CoV-2-specific TCR repertoires in individuals who recovered from mild

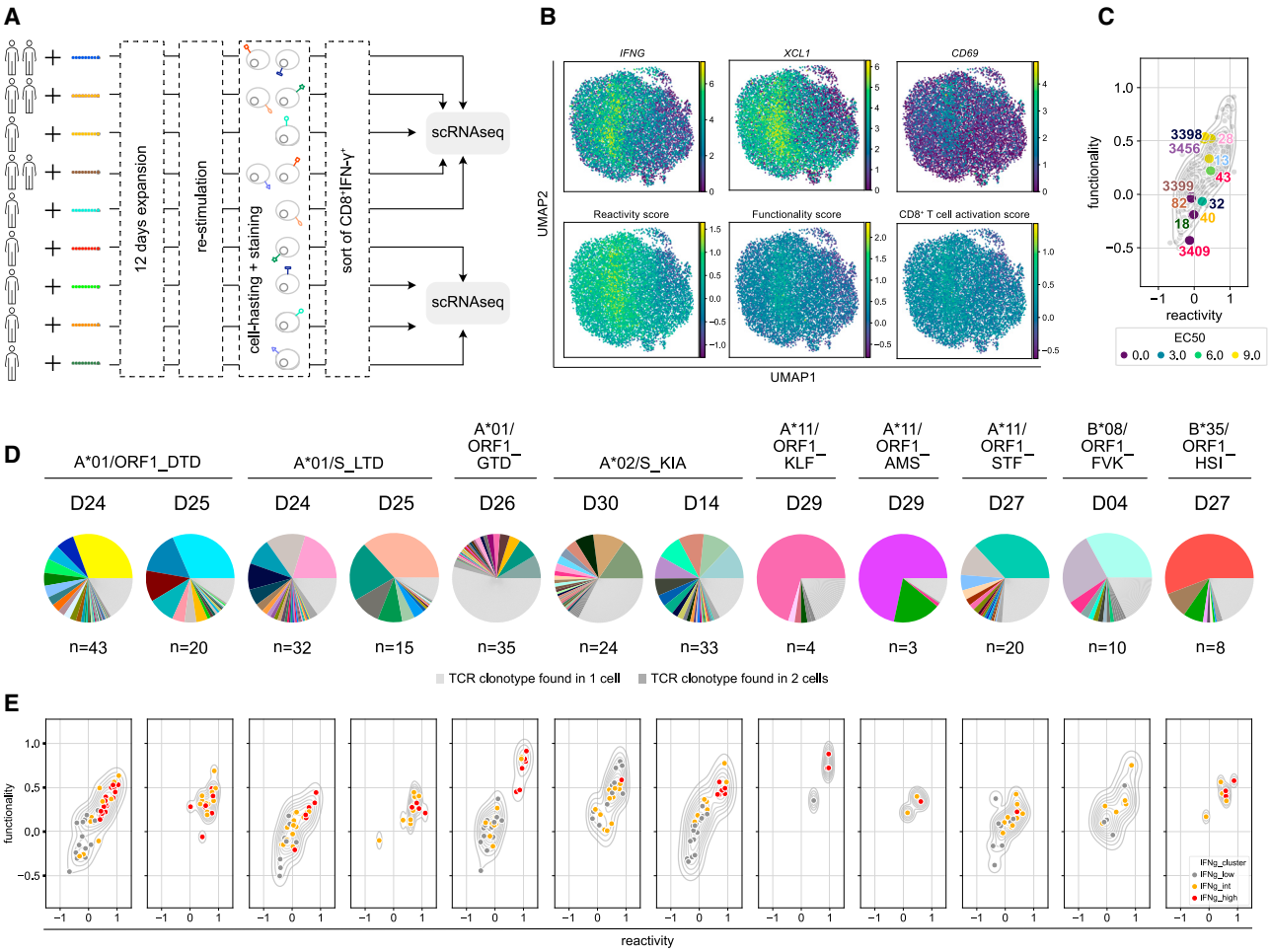

Figure 6. Functional TCRs are recruited in non-severe SARS-CoV-2 infections

(A) Schematic of the experimental setup.

(B) UMAP neighborhood embedding showing distribution of T cell function and activation marker expression across the dataset.

(C) TCR clonotype distribution according to reactivity score and functionality score. Functionally validated TCRs from Figure 5 were overlaid as a benchmark. Contours show KDEs of the dataset, and dot color corresponds to the IFN-γ EC_{50} of the validated TCRs.

(D) Pie chart showing the percentage of each TCR clonotype of the total repertoire for the individual peptides and donors.

(E) TCR clonotype distribution according to reactivity score and functionality score for the individual peptides and donors. Contours show KDEs for each individual sample, and the color code corresponds to the IFNG expression batches (low, intermediate, high).

symptomatic disease. First we learned that, in this clinical situation, SARS-CoV-2 epitope-specific $CD8^+$ T cells are very low in frequency in peripheral blood and difficult to detect *ex vivo* from a limited sample size. However, a short step of peptide-mediated *in vitro* expansion (Oh et al., 2011) allowed us to robustly detect SARS-CoV-2-specific $CD8^+$ T cells in convalescent individuals, similar to other studies (Nelde et al., 2020; Schulien et al., 2020; Shomuradova et al., 2020).

By combining this *in vitro* peptide expansion with scRNA-seq, we accessed the HLA class I-restricted TCR repertoire specific toward immunodominant and therefore relevant SARS-CoV-2 epitopes. Beside validation of SARS-CoV-2 specificity and peptide sensitivity, of particular importance and unique from other studies (Francis et al., 2021) was the experimental validation that TCRs with high sensitivity toward SARS-CoV-2-specific epitopes can mediate cytotoxicity against virus-infected cells. The association between immunogenicity (the ability of eliciting an immune response) and protection (the direct contribution to the resolution of infection by the elicited immune response) is not self-explanatory. Immunogenic epitopes can be efficiently cross-presented but eventually not expressed in infected target cells (Holtappels et al., 2004; Kienzle et al., 1998), in particular for *in-silico*-predicted epitopes (Willimsky et al., 2021), inducing T cell responses that are neither relevant nor indicative of the course of the infection. For two epitopes (A1/ORF3a_FTS or A3/ORF1_VTN), we showed that T cells genetically engineered with SARS-CoV-2-specific TCRs were capable of directly killing virus-infected cells *in vitro* through specific epitope recognition. This evidence gives an additional value to the epitopes under investigation. Besides immunogenicity and immunodominance, which have been corroborated widely by other studies where the landscape of HLA class I-restricted SARS-CoV-2 epitopes

was exhaustively deciphered (Quadeer et al., 2021), the epitopes we described are indicative of recruitment of highly functional $CD8^+$ T cell responses. Thus, they are particularly useful tools for studying the quality of T cell responses in several contexts; e.g., after vaccination and severe infection.

Identification of functional and highly effective SARS-CoV-2-specific TCRs also opens up possibilities for therapeutic use based on TCR-engineered T cells in individuals with high risk of developing a severe clinical course. The therapeutic value of adoptive transfer of antigen-specific, TCR-engineered T cells is well recognized (D'Ippolito et al., 2019, 2020), especially now that precise genetic engineering offers the flexibility of generating increasingly sophisticated but near-physiological autologous T cell products (Schober et al., 2019). Furthermore, accumulated evidence supports a model where late recruitment of T cells (Tan et al., 2021), presumably because of delayed activation of the type I IFN response (Combes et al., 2021), contributes to disease progression, offering a therapeutic window for adoptive transfer of potentially curative TCR-engineered T cells. Recent findings also disproved initial concerns about the potential role of T cells in immunopathology in advanced COVID-19, attributed to the massive amount of lung-infiltrating neutrophils and circulating monocytes (Park and Lee, 2020).

A limitation of our study is the use of an *in vitro* expansion step prior T cell analyses, which may bias the relative abundance of clonotypes and may favor outgrowing of some clones at the expense of others. However, this approach of peptide stimulation offered the possibility of exploiting signatures of recent activation to discriminate epitope-specific and functional TCRs (Fischer et al., 2021). Indeed, we identified signatures of T cell function and recent activation correlating with TCR functionality, which allowed a broad *in silico* investigation of the functional landscape of entire TCR repertoires, which is otherwise unfeasible by conventional experimental validation. Remarkably, we predicted highly functional TCRs for each of the eleven immunodominant SARS-CoV-2 epitopes analyzed, despite a certain degree of functional heterogeneity. Together with the observed polyclonality, our data indicate that functional and diverse $CD8^+$ T cell immunity should establish normally in non-severe SARS-CoV-2 infection. Polyclonality and high functionality are hallmarks of a protective TCR repertoire (Song et al., 2017), strongly supporting a similar role in the context of SARS-CoV-2 infection. Nevertheless, extension of TCR repertoire analyses to settings of severe infection remains a fundamental next step to assign $CD8^+$ T cell responses a role as correlates of protection.

Overall, our data provide first evidence that SARS-CoV-2-specific $CD8^+$ T cells persists up to 12 months after infection and are composed of a polyclonal and highly functional TCR repertoire capable of mediating direct killing of virus-infected cells. In addition, we provide tools—epitopes and TCRs—indicative of functional responses, useful for appropriately investigating and potentially diagnosing correlates of protection in individuals with severe disease.

Limitations of the study

In this study, we limited selection of SARS-CoV-2 epitopes according to the most common HLA class I molecules in the Caucasian population. The study was conducted in Germany, and because of the ongoing pandemic, we were restricted to blood samples from local hospitals. Therefore, representation of other races was limited. Continuous epitope discovery for additional HLAs is necessary to broadly apply our findings to other ethnicities. Further, individuals with severe disease were not included in this study, precluding conclusive statements regarding the role of $CD8^+$ T cells in protection. Finally, all of our experiments relied on a step of *in vitro* expansion, which biased the original phenotype and frequency of SARS-CoV-2-specific T cells. In particular, when analyzing individuals with severe disease, *ex vivo* TCR repertoire analyses combined with phenotype assessments may provide a unique setting to clarify the quality of cytotoxic $CD8^+$ T cells in severe COVID-19.

STAR★METHODS

Detailed methods are provided in the online version of this paper and include the following:

- KEY RESOURCES TABLE
- RESOURCE AVAILABILITY
  - Lead contact
  - Materials availability
  - Data and code availability
- EXPERIMENTAL MODEL AND SUBJECT DETAILS
  - Clinical samples
  - Human primary T cells from whole blood and cell culture
- METHODS DETAILS
  - Detection of SARS-CoV-2 adaptive immunity
  - Single-cell RNA sequencing and data analyses
  - TCR re-expression and functional validation
- QUANTIFICATION AND STATISTICAL ANALYSIS

SUPPLEMENTAL INFORMATION

Supplemental information can be found online at https://doi.org/10.1016/j.celrep.2021.110214.

ACKNOWLEDGMENTS

We thank Max Koch for processing blood for PBMCs isolation and Noomen Hamed for the production of HLA multimers. We gratefully acknowledge Catharina Gerhards, Margot Thiaucourt, and Laura Mirbach for contributions to the logistics organization of blood sample delivery.

This study was supported by the EIT Health CoViproteHCt 20877, the German National Network of University Medicine of the Federal Ministry of Education and Research (BMBF; NaFoUniMedCovid19, 01KX2021; COVIM), and the Deutsche Forschungsgesellschaft (DFG; German Research Foundation) SFB1321/1-329628492 (project P17) and SFB-TRR 338/1 2021-452881907 (project A01). E.D. was funded by the Corona-Forschungsanträge (Fakultät für Medizin). The work in the laboratory of A. Pichlmair was funded by an ERC consolidator grant (ERC-CoG ProDAP, 817798), the German Federal Ministry of Education and Research (COVINET), the German Research Foundation (PI 1084/5 and TRR179, TRR237), and the Bavarian State Ministry of Science and Arts (Bavarian Research Network FOR-COVID). L.M.M. was supported by a Ph.D. fellowship from the Boehringer Ingelheim Fonds.

AUTHOR CONTRIBUTIONS

D.H.B. and E.D. conceptualized the study. K.I.W. and L.M.M. performed experiments. K.I.W., L.M.M., S.J., and E.D. performed software analyses. V.G.

and A. Pichlmair. performed killing assays. C.S.C. and M.G. designed and implemented the study on mild COVID-19. H.P., H.B., S.S., S.H., A.S.-A., V.H., and M.N. collected blood samples and clinical information from individuals with mild COVID-19. U.P., P.A.K., J.E., A.P., S.Y., and H.R. designed and organized the study on asymptomatic donors. M.O. and T.T. provided prepandemic biosamples. K.W. performed HLA genotyping. T.B. and B.K. performed serology analyses. S.W., M.H., and H.M. contributed resources. D.H.B. and E.D. wrote the manuscript. K.I.W., L.M.M., S.J., and E.D. prepared figures. All authors read and approved the manuscript. D.H.B., M.G., C.S.C., K.S., and E.D. acquired funding. D.H.B. and E.D. supervised the study and administered the project.

DECLARATION OF INTERESTS

D.H.B. is co-founder of STAGE Cell Therapeutics GmbH (now Juno Therapeutics/Celgene) and T cell Factory B.V. (now Kite/Gilead). D.H.B. has a consulting contract with and receives sponsored research support from Juno Therapeutics, a Bristol Myers Squibb Company.

Received: August 27, 2021
Revised: November 7, 2021
Accepted: December 13, 2021
Published: December 17, 2021

REFERENCES

Addetia, A., Crawford, K.H.D., Dingens, A., Zhu, H., Roychoudhury, P., Huang, M.-L., Jerome, K.R., Bloom, J.D., and Greninger, A.L. (2020). Neutralizing antibodies correlate with protection from SARS-CoV-2 in humans during a fishery vessel outbreak with a high attack rate. J. Clin. Microbiol. *58*. https://doi.org/10.1128/JCM.02107-20.

Bacher, P., Rosati, E., Esser, D., Martini, G.R., Saggau, C., Schiminsky, E., Dargvainiene, J., Schöder, I., Wieters, I., Khodamoradi, Y., et al. (2020). Low avidity CD4+ T cell responses to SARS-CoV-2 in unexposed individuals and humans with severe COVID-19. Immunity *53*, 1258–1271.

Braun, J., Loyal, L., Frentsch, M., Wendisch, D., Georg, P., Kurth, F., Hippenstiel, S., Dingeldey, M., Kruse, B., Fauchere, F., et al. (2020). SARS-CoV-2-reactive T cells in healthy donors and patients with COVID-19. Nature *587*, 270–274.

Brewitz, A., Eickhoff, S., Dähling, S., Quast, T., Bedoui, S., Kroczek, R.A., Kurts, C., Garbi, N., Barchet, W., Iannacone, M., et al. (2017). CD8+ T cells orchestrate pDC-XCR1+ dendritic cell spatial and functional cooperativity to optimize priming. Immunity *46*, 205–219.

Busch, D.H., and Pamer, E.G. (1999). T cell affinity maturation by selective expansion during infection. J. Exp. Med. *189*, 701–710.

Callan, M.F., Steven, N., Krausa, P., Wilson, J.D., Moss, P.A., Gillespie, G.M., Bell, J.I., Rickinson, A.B., and McMichael, A.J. (1996). Large clonal expansions of CD8+ T cells in acute infectious mononucleosis. Nat. Med. *2*, 906–911.

Channappanavar, R., Fett, C., Zhao, J., Meyerholz, D.K., and Perlman, S. (2014). Virus-specific memory CD8 T cells provide substantial protection from lethal severe acute respiratory syndrome coronavirus infection. J. Virol. *88*, 11034–11044.

Cohen, C.J., Li, Y.F., El-Gamil, M., Robbins, P.F., Rosenberg, S.A., and Morgan, R.A. (2007). Enhanced antitumor activity of T cells engineered to express T-cell receptors with a second disulfide bond. Cancer Res. *67*, 3898–3903.

Combes, A.J., Courau, T., Kuhn, N.F., Hu, K.H., Ray, A., Chen, W.S., Chew, N.W., Cleary, S.J., Kushnoor, D., Reeder, G.C., et al. (2021). Global absence and targeting of protective immune states in severe COVID-19. Nature *591*, 124–130.

D'Ippolito, E., Schober, K., Nauerth, M., and Busch, D.H. (2019). T cell engineering for adoptive T cell therapy: safety and receptor avidity. Cancer Immunol. Immunother. *68*, 1701–1712.

D'Ippolito, E., Wagner, K.I., and Busch, D.H. (2020). Needle in a haystack: the naïve repertoire as a source of T cell receptors for adoptive therapy with engineered T cells. Int. J. Mol. Sci. *21*, 1–24.

Dan, J.M., Mateus, J., Kato, Y., Hastie, K.M., Yu, E.D., Faliti, C.E., Grifoni, A., Ramirez, S.I., Haupt, S., Frazier, A., et al. (2021). Immunological memory to SARS-CoV-2 assessed for up to 8 months after infection. Science *371*, eabf4063.

Deng, W., Bao, L., Liu, J., Xiao, C., Liu, J., Xue, J., Lv, Q., Qi, F., Gao, H., Yu, P., et al. (2020). Primary exposure to SARS-CoV-2 protects against reinfection in rhesus macaques. Science *369*, 818–823.

Effenberger, M., Stengl, A., Schober, K., Gerget, M., Kampick, M., Müller, T.R., Schumacher, D., Helma, J., Leonhardt, H., and Busch, D.H. (2019). FLEXamers: a double tag for universal generation of versatile peptide-MHC multimers. J. Immunol. *202*, 2164–2171.

Ferretti, A.P., Kula, T., Wang, Y., Nguyen, D.M.V., Weinheimer, A., Dunlap, G.S., Xu, Q., Nabilsi, N., Perullo, C.R., Cristofaro, A.W., et al. (2020). Unbiased screens show CD8(+) T cells of COVID-19 patients recognize shared epitopes in SARS-CoV-2 that largely reside outside the Spike protein. Immunity *53*, 1095–1107.e3.

Fischer, D.S., Ansari, M., Wagner, K.I., Jarosch, S., Huang, Y., Mayr, C.H., Strunz, M., Lang, N.J., D'Ippolito, E., Hammel, M., et al. (2021). Single-cell RNA sequencing reveals ex vivo signatures of SARS-CoV-2-reactive T cells through 'reverse phenotyping'. Nat. Commun. *12*, 4515.

Flynn, K.J., Belz, G.T., Altman, J.D., Ahmed, R., Woodland, D.L., and Doherty, P.C. (1998). Virus-specific CD8+ T cells in primary and secondary influenza pneumonia. Immunity *8*, 683–691.

Francis, J.M., Leistritz-Edwards, D., Dunn, A., Tarr, C., Lehman, J., Dempsey, C., Hamel, A., Rayon, V., Liu, G., Wang, Y., et al. (2021). Allelic variation in class I HLA determines CD8+ T cell repertoire shape and cross-reactive memory responses to SARS-CoV-2. Sci. Immunol. *3070*, eabk3070.

Grifoni, A., Weiskopf, D., Ramirez, S.I., Mateus, J., Dan, J.M., Moderbacher, C.R., Rawlings, S.A., Sutherland, A., Premkumar, L., Jadi, R.S., et al. (2020). Targets of T Cell responses to SARS-CoV-2 coronavirus in humans with COVID-19 disease and unexposed individuals. Cell *181*, 1489–1501.e15.

Grossman, W.J., Verbsky, J.W., Tollefsen, B.L., Kemper, C., Atkinson, J.P., and Ley, T.J. (2004). Differential expression of granzymes A and B in human cytotoxic lymphocyte subsets and T regulatory cells. Blood *104*, 2840–2848.

Habel, J.R., Nguyen, T.H.O., van de Sandt, C.E., Juno, J.A., Chaurasia, P., Wragg, K., Koutsakos, M., Hensen, L., Jia, X., Chua, B., et al. (2020). Suboptimal SARS-CoV-2–specific CD8+ T cell response associated with the prominent HLA-A*02:01 phenotype. Proc. Natl. Acad. Sci. U S A *117*, 24384–24391.

Hall, V.J., Foulkes, S., Charlett, A., Atti, A., Monk, E.J.M., Simmons, R., Wellington, E., Cole, M.J., Saei, A., Oguti, B., et al. (2021). SARS-CoV-2 infection rates of antibody-positive compared with antibody-negative health-care workers in England: a large, multicentre, prospective cohort study (SIREN). Lancet *397*, 1459–1469.

Hansen, C.H., Michlmayr, D., Gubbels, S.M., Mølbak, K., and Ethelberg, S. (2021). Assessment of protection against reinfection with SARS-CoV-2 among 4 million PCR-tested individuals in Denmark in 2020: a population-level observational study. Lancet *397*, 1204–1212.

Heaton, H., Talman, A.M., Knights, A., Imaz, M., Gaffney, D.J., Durbin, R., Hemberg, M., and Lawniczak, M.K.N. (2020). Souporcell: robust clustering of single-cell RNA-seq data by genotype without reference genotypes. Nat. Methods *17*, 615–620.

Heidema, J., Rossen, J.W.A., Lukens, M.V., Ketel, M.S., Scheltens, E., Kranendonk, M.E.G., van Maren, W.W.C., van Loon, A.M., Otten, H.G., Kimpen, J.L.L., et al. (2008). Dynamics of human respiratory virus-specific CD8 + T cell responses in blood and airways during episodes of common cold. J. Immunol. *181*, 5551–5559.

Holtappels, R., Podlech, J., Pahl-Seibert, M.F., Jülch, M., Thomas, D., Simon, C.O., Wagner, M., and Reddehase, M.J. (2004). Cytomegalovirus misleads its host by priming of CD8 T cells specific for an epitope not presented in infected tissues. J. Exp. Med. *199*, 131–136.

Huster, K.M., Stemberger, C., and Busch, D.H. (2006). Protective immunity towards intracellular pathogens. Curr. Opin. Immunol. *18*, 458–464.

Jozwik, A., Habibi, M.S., Paras, A., Zhu, J., Guvenel, A., Dhariwal, J., Almond, M., Wong, E.H.C., Sykes, A., Maybeno, M., et al. (2015). RSV-specific airway resident memory CD8+ T cells and differential disease severity after experimental human infection. Nat. Commun. *6*, 10224.

Jung, J.H., Rha, M.-S., Sa, M., Choi, H.K., Jeon, J.H., Seok, H., Park, D.W., Park, S.-H., Jeong, H.W., Choi, W.S., et al. (2021). SARS-CoV-2-specific T cell memory is sustained in COVID-19 convalescent patients for 10 months with successful development of stem cell-like memory T cells. Nat. Commun. *12*, 1–12.

Kienzle, N., Sculley, T.B., Poulsen, L., Buck, M., Cross, S., Raab-Traub, N., and Khanna, R. (1998). Identification of a cytotoxic T-lymphocyte response to the novel BARF0 protein of epstein-Barr virus: a critical role for antigen expression. J. Virol. *72*, 6614–6620.

Le Bert, N., Tan, A.T., Kunasegaran, K., Tham, C.Y.L., Hafezi, M., Chia, A., Chng, M.H.Y., Lin, M., Tan, N., Linster, M., et al. (2020). SARS-CoV-2-specific T cell immunity in cases of COVID-19 and SARS, and uninfected controls. Nature *584*, 457–462.

Lin, L., Couturier, J., Yu, X., Medina, M.A., Kozinetz, C.A., and Lewis, D.E. (2014). Granzyme B secretion by human memory CD4 T cells is less strictly regulated compared to memory CD8 T cells. BMC Immunol. *15*, 1–15.

Lukacher, A.E., Braciale, V.L., and Braciale, T.J. (1984). In vivo effector function of influenza virus-specific cytotoxic T lymphocyte clones is highly specific. J. Exp. Med. *160*, 814–826.

Lukens, M.V., Claassen, E.A.W., de Graaff, P.M.A., van Dijk, M.E.A., Hoogerhout, P., Toebes, M., Schumacher, T.N., van der Most, R.G., Kimpen, J.L.L., and van Bleek, G.M. (2006). Characterization of the CD8+ T cell responses directed against respiratory syncytial virus during primary and secondary infection in C57BL/6 mice. Virology *352*, 157–168.

Lumley, S.F., O'Donnell, D., Stoesser, N.E., Matthews, P.C., Howarth, A., Hatch, S.B., Marsden, B.D., Cox, S., James, T., Warren, F., et al. (2021). Antibody status and incidence of SARS-CoV-2 infection in health care workers. N. Engl. J. Med. *384*, 533–540.

Mateus, J., Grifoni, A., Tarke, A., Sidney, J., Ramirez, S.I., Dan, J.M., Burger, Z.C., Rawlings, S.A., Smith, D.M., Phillips, E., et al. (2020). Selective and cross-reactive SARS-CoV-2 T cell epitopes in unexposed humans. Science *370*, 89–94.

Mathew, D., Giles, J.R., Baxter, A.E., Oldridge, D.A., Greenplate, A.R., Wu, J.E., Alanio, C., Kuri-Cervantes, L., Pampena, M.B., D'Andrea, K., et al. (2020). Deep immune profiling of COVID-19 patients reveals distinct immunotypes with therapeutic implications. Science *369*, eabc8511.

McMahan, K., Yu, J., Mercado, N.B., Loos, C., Tostanoski, L.H., Chandrashekar, A., Liu, J., Peter, L., Atyeo, C., Zhu, A., et al. (2021). Correlates of protection against SARS-CoV-2 in rhesus macaques. Nature *590*, 630–634.

Nelde, A., Bilich, T., Heitmann, J.S., Maringer, Y., Salih, H.R., Roerden, M., Lübke, M., Bauer, J., Rieth, J., Wacker, M., et al. (2020). SARS-CoV-2-derived peptides define heterologous and COVID-19-induced T cell recognition. Nat. Immunol. *22*, 74–85.

Nguyen, T.H.O., Rowntree, L.C., Petersen, J., Chua, B.Y., Hensen, L., Kedzierski, L., van de Sandt, C.E., Chaurasia, P., Tan, H.X., Habel, J.R., et al. (2021). CD8+ T cells specific for an immunodominant SARS-CoV-2 nucleocapsid epitope display high naive precursor frequency and TCR promiscuity. Immunity *54*, 1066–1082.e5.

Niessl, J., Sekine, T., Lange, J., Konya, V., Forkel, M., Maric, J., Rao, A., Mazzurana, L., Kokkinou, E., Weigel, W., et al. (2021). Identification of resident memory CD8 + T cells with functional specificity for SARS-CoV-2 in unexposed oropharyngeal lymphoid tissue. Sci. Immunol. *6*, eabk0894.

Oh, H.-L.J., Chia, A., Chang, C.X.L., Leong, H.N., Ling, K.L., Grotenbreg, G.M., Gehring, A.J., Tan, Y.J., and Bertoletti, A. (2011). Engineering T cells specific for a dominant severe acute respiratory syndrome coronavirus CD8 T cell epitope. J. Virol. *85*, 10464–10471.

Park, J.H., and Lee, H.K. (2020). Re-analysis of single cell transcriptome reveals that the NR3C1-CXCL8-neutrophil Axis determines the severity of COVID-19. Front. Immunol. *11*, 1–9.

Patiño-Lopez, G., Hevezi, P., Lee, J., Willhite, D., Verge, G.M., Lechner, S.M., Ortiz-Navarrete, V., and Zlotnik, A. (2006). Human class-I restricted T cell associated molecule is highly expressed in the cerebellum and is a marker for activated NKT and CD8+ T lymphocytes. J. Neuroimmunol. *171*, 145–155.

Peng, Y., Mentzer, A.J., Liu, G., Yao, X., Yin, Z., Dong, D., Dejnirattisai, W., Rostron, T., Supasa, P., Liu, C., et al. (2020). Broad and strong memory CD4+ and CD8+ T cells induced by SARS-CoV-2 in UK convalescent individuals following COVID-19. Nat. Immunol. *21*, 1336–1345.

Quadeer, A.A., Ahmed, S.F., and McKay, M.R. (2021). Landscape of epitopes targeted by T cells in 852 individuals recovered from COVID-19: meta-analysis, immunoprevalence, and web platform. Cell Rep. Med. *2*, 100312.

Rojas-Marquez, C., Valle-Rios, R., Lopez-Bayghen, E., and Ortiz-Navarrete, V. (2015). CRTAM is negatively regulated by ZEB1 in T cells. Mol. Immunol. *66*, 290–298.

Rydyznski Moderbacher, C., Ramirez, S.I., Dan, J.M., Grifoni, A., Hastie, K.M., Weiskopf, D., Belanger, S., Abbott, R.K., Kim, C., Choi, J., et al. (2020). Antigen-specific adaptive immunity to SARS-CoV-2 in acute COVID-19 and associations with age and disease severity. Cell *183*, 996–1012.e19.

Schober, K., Müller, T.R., Gökmen, F., Grassmann, S., Effenberger, M., Poltorak, M., Stemberger, C., Schumann, K., Roth, T.L., Marson, A., et al. (2019). Orthotopic replacement of T-cell receptor α- and β-chains with preservation of near-physiological T-cell function. Nat. Biomed. Eng. *3*, 974–984.

Schulien, I., Kemming, J., Oberhardt, V., Wild, K., Seidel, L.M., Killmer, S., Sagar, Daul, F., Salvat Lago, M., Decker, A., et al. (2020). Characterization of pre-existing and induced SARS-CoV-2-specific CD8+ T cells. Nat. Med. *27*, 78–85.

Sekine, T., Rivera-Ballesteros, O., Ljunggren, H., Aleman, S., Buggert, M., Parrot, T., and Folkesson, E.; Karolinska COVID-19 Study Group (2020). Robust T cell immunity in convalescent individuals with asymptomatic or mild COVID-19. Cell *183*, 158–168.

Sherina, N., Piralla, A., Du, L., Wan, H., Kumagai-Braesch, M., Andréll, J., Braesch-Andersen, S., Cassaniti, I., Percivalle, E., Sarasini, A., et al. (2021). Persistence of SARS-CoV-2-specific B and T cell responses in convalescent COVID-19 patients 6–8 months after the infection. Med (N Y) *2*, 281–295.e4.

Shomuradova, A.S., Vagida, M.S., Sheetikov, S.A., Zornikova, K.V., Kiryukhin, D., Titov, A., Peshkova, I.O., Khmelevskaya, A., Dianov, D.V., Malasheva, M., et al. (2020). SARS-CoV-2 epitopes are recognized by a public and diverse repertoire of human T cell receptors. Immunity *53*, 1245–1257.e5.

Sokal, A., Chappert, P., Barba-Spaeth, G., Roeser, A., Fourati, S., Azzaoui, I., Vandenberghe, A., Fernandez, I., Meola, A., Bouvier-Alias, M., et al. (2021). Maturation and persistence of the anti-SARS-CoV-2 memory B cell response. Cell *184*, 1201–1213.e14.

Song, I.Y., Gil, A., Mishra, R., Ghersi, D., Selin, L.K., and Stern, L.J. (2017). Broad TCR repertoire and diverse structural solutions for recognition of an immunodominant CD8+ T cell epitope. Nat. Struct. Mol. Biol. *24*, 395–406.

Soresina, A., Moratto, D., Chiarini, M., Paolillo, C., Baresi, G., Focà, E., Bezzi, M., Baronio, B., Giacomelli, M., and Badolato, R. (2020). Two X-linked agammaglobulinemia patients develop pneumonia as COVID-19 manifestation but recover. Pediatr. Allergy Immunol. *31*, 565–569.

Stukalov, A., Girault, V., Grass, V., Karayel, O., Bergant, V., Urban, C., Haas, D.A., Huang, Y., Oubraham, L., Wang, A., et al. (2021). Multilevel proteomics reveals host perturbations by SARS-CoV-2 and SARS-CoV. Nature *594*, 246–252.

Sturm, G., Szabo, T., Fotakis, G., Haider1, M., Rieder, D., Trajanoski, Z., and Finotello, F. (2020). Scirpy: a Scanpy extension for analyzing single-cell T-cell receptor-sequencing data. Bioinformatics *36*, 4817–4818.

Suthar, M.S., Zimmerman, M.G., Kauffman, R.C., Mantus, G., Linderman, S.L., Hudson, W.H., Vanderheiden, A., Nyhoff, L., Davis, C.W., Adekunle, O., et al. (2020). Rapid generation of neutralizing antibody responses in COVID-19 patients. Cell Rep. Med. *1*, 100040.

Sylwester, A.W., Mitchell, B.L., Edgar, J.B., Taormina, C., Pelte, C., Ruchti, F., Sleath, P.R., Grabstein, K.H., Hosken, N.A., Kern, F., et al. (2005). Broadly targeted human cytomegalovirus-specific CD4+ and CD8+ T cells dominate the memory compartments of exposed subjects. J. Exp. Med. *202*, 673–685.

Tan, A.T., Linster, M., Tan, C.W., Le Bert, N., Chia, W.N., Kunasegaran, K., Zhuang, Y., Tham, C.Y.L., Chia, A., Smith, G.J.D., et al. (2021). Early induction of functional SARS-CoV-2-specific T cells associates with rapid viral clearance and mild disease in COVID-19 patients. Cell Rep. *34*, 108728.

Tarke, A., Sidney, J., Kidd, C.K., Dan, J.M., Ramirez, S.I., Yu, E.D., Mateus, J., da Silva Antunes, R., Moore, E., Rubiro, P., et al. (2021). Comprehensive analysis of T cell immunodominance and immunoprevalence of SARS-CoV-2 epitopes in COVID-19 cases. Cell Rep. Med. *2*, 100204.

Thi Nhu Thao, T., Labroussaa, F., Ebert, N., V'kovski, P., Stalder, H., Portmann, J., Kelly, J., Steiner, S., Holwerda, M., Kratzel, A., et al. (2020). Rapid reconstruction of SARS-CoV-2 using a synthetic genomics platform. Nature *582*, 561–565.

Wang, Z., Yang, X., Zhong, J., Zhou, Y., Tang, Z., Zhou, H., He, J., Mei, X., Tang, Y., Lin, B., et al. (2021). Exposure to SARS-CoV-2 generates T-cell memory in the absence of a detectable viral infection. Nat. Commun. *12*, 6–13.

Willimsky, G., Beier, C., Immisch, L., Papafotiou, G., Scheuplein, V., Goede, A., Holzhütter, H.G., Blankenstein, T., and Kloetzel, P.M. (2021). In vitro proteasome processing of neo-splicetopes does not predict their presentation in vivo. Elife *10*, 1–22.

Wolf, F.A., Angerer, P., and Theis, F.J. (2018). SCANPY: large-scale single-cell gene expression data analysis. Genome Biol. *19*, 15.

Xu, J., Falconer, C., Nguyen, Q., Crawford, J., McKinnon, B.D., Mortlock, S., Senabouth, A., Andersen, S., Chiu, H.S., Jiang, L., et al. (2019). Genotype-free demultiplexing of pooled single-cell RNA-seq. Genome Biol. *20*, 1–12.

Yap, K.L., Ada, G.L., and McKenzie, I.F.C. (1978). Transfer of specific cytotoxic T lymphocytes protects mice inoculated with influenza virus. Nature *273*, 238–239.

Yeh, J.H., Sidhu, S.S., and Chan, A.C. (2008). Regulation of a late phase of T cell polarity and effector functions by crtam. Cell *132*, 846–859.

Zehn, D., Lee, S.Y., and Bevan, M.J. (2009). Complete but curtailed T-cell response to very low-affinity antigen. Nature *458*, 211–214.

Zhou, P., Yang, X.-L., Wang, X.G., Hu, B., Zhang, L., Zhang, W., Si, H.R., Zhu, Y., Li, B., Huang, C.L., et al. (2020). A pneumonia outbreak associated with a new coronavirus of probable bat origin. Nature *579*, 270–273.

Zhu, N., Zhang, D., Wang, W., Li, X., Yang, B., Song, J., Zhao, X., Huang, B., Shi, W., Lu, R., et al. (2020). A novel coronavirus from patients with pneumonia in China, 2019. N. Engl. J. Med. *382*, 727–733.

Zuo, J., Dowell, A.C., Pearce, H., Verma, K., Long, H.M., Begum, J., Aiano, F., Amin-Chowdhury, Z., Hallis, B., Stapley, L., et al. (2021). Robust SARS-CoV-2-specific T cell immunity is maintained at 6 months following primary infection. Nat. Immunol. *22*, 620–626.

STAR★METHODS

KEY RESOURCES TABLE

REAGENT or RESOURCE	SOURCE	IDENTIFIER
Antibodies		
CD19-ECD (J3-119)	Beckman Coulter	Cat# A07770
CD3-BV421 (SK7)	BD Biosciences	Cat# 659448; RRID:AB_2870486
CD3-PC7 (UCHT.1)	Beckman Coulter	Cat# 737657; RRID:AB_2636813
CD8-eF450 (OKT8)	Life Technologies	Cat# 48-0086-42; RRID:AB_1907412
CD8-FITC (B9.11)	Beckman Coulter	Cat# A07756; RRID:AB_1575981
CD8-PE (3B5)	Life Technologies	Cat# MHCD0804; RRID:AB_10372952
HLA-A*02-FITC	BD Biosciences	Cat# 551285; RRID:AB_394130
HLA-A*03-APC	Miltenyi	Cat# 130-115-795; RRID:AB_2727192
HLA-B*07-PE	Biolegend	Cat# 372404; RRID:AB_2650774
HLA-B*08-APCVio770	Miltenyi	Cat# 130-099-5910
IFN-γ catch	Miltenyi	Cat# 130-090-433
IFN-γ FITC (25723.11)	BD Biosciences	Cat# 340449; RRID:AB_400425
mTRBC-APC/Fire750 (H57-597)	Biolegend	Cat# 109246; RRID:AB_2629697
mTRBC-PE (h57-597)	Biolegend	Cat# 109208; RRID:AB_313431
Streptavidin-APC	eBioscience	Cat# 17-4317-82
Total Seq-C 0251 (10x Hashtaq 1)	Biolegend	Cat# 394661; RRID:AB_2801031
Total Seq-C 0252 (10x Hashtaq 2)	Biolegend	Cat# 394663; RRID:AB_2801032
Total Seq-C 0253 (10x Hashtaq 3)	Biolegend	Cat# 394665; RRID:AB_2801033
Total Seq-C 0254 (10x Hashtaq 4)	Biolegend	Cat# 394667; RRID:AB_2801034
Total Seq-C 0255 (10x Hashtaq 5)	Biolegend	Cat# 394669; RRID:AB_2801035
Total Seq-C 0256 (10x Hashtaq 6)	Biolegend	Cat# 394671; RRID:AB_2820042
Bacterial and virus strains		
Stbl3	Thermo Fisher Scientific	Cat# C737303
SARS-CoV-2 GFP	In house production	N/A
Biological samples		
Human PBMCs convalescent mild COVID19	In house	N/A
Chemicals, peptides, and recombinant proteins		
RPMI 1640 Gibco	Sigma	Cat# R0883
Agencourt CleanSeq magnetic beads	Beckman Coulter	Cat# A63881
Alt-R® Cas9 Electroporation Enhancer	IDT	Cat# 1075916
Alt-R® S.p. HiFi Cas9 Nuclease V3	IDT	Cat# 1081061
Ampicillin	Roth	Cat# K029.1
BigDye®Terminator v3.1 Cycle Sequencing RR-100	Applied Biosystems	Cat# 4337458
Cytofix/Cytoperm	BD Biosciences	Cat# 554714
DBCO-PEG4-Biotin	Jena Bioscience	Cat# CLK-A105P4-10
DMEM	Life Technologies	Cat# 10938025
DMSO	Merck	Cat# D8418
DNA LoBind tubes	Sigma	Cat# EP0030108051, EP0030108078, EP0030124359
Ethidium Monoazide Bromide (EMA)	Life Technologies	Cat# E1374
Fetal calf serum	Biochrom	N/A

(*Continued on next page*)

Continued

REAGENT or RESOURCE	SOURCE	IDENTIFIER
Fibronectin	Sigma	Cat# F2006
Gentamicin	Life Technologies	Cat# 15750-037
GolgiPlug	BD Biosciences	Cat# 555029
HEPES	Life Technologies	Cat# 15630056
Human serum	In house	N/A
Ionomycin	Sigma	Cat# I9657
LB-medium / agar	In house	N/A
L-Glutamine	Sigma	Cat# G8540-100G
Pancoll human (1.077g/ml)	PAN Biotech	Cat# P04-601000
Penicillin/Streptomycin	Life Technologies	Cat# 10378016
PepTivator SARS-CoV-2 Protein S	Miltenyi	Cat# 130-126-701
Phorbol myristate acetate	Sigma	Cat# P1585
Propidium Iodide (PI)	Life Technologies	Cat# P1304MP
Q-solution	Qiagen	Cat# 201203
Recombinant human IL-15	Peprotech	Cat# 200-15
Recombinant human IL-2	Peprotech	Cat# 200-02
Recombinant human IL-7	Peprotech	Cat# 200-07
Retronectin	TaKaRa	Cat# T100B
RPT filter tips	Starlab	Cat# S1183-1710, SS1180-8710, S1182-1730
SARS-CoV-2 individual peptides	IBA	N/A
SARS-CoV-2 individual peptides	peptides & elephants	N/A
β-mercaptoethanol	Life Technologies	Cat# 31350010
Critical commercial assays		
iFlash SARS-CoV-2 IgG (2019-nCov IgG)	SHENZHEN YHLO BIOTECH CO	Cat# C86095G
Agencout AMPure XP	Beckman Coulter	Cat# A63881
High sensitivity DNA Kit	Agilent	Cat# 5067-4626
P3 Primary Cell Kit	Lonza	Cat# V4XP-3024 V4XP-3096
Qubit dsDNA hs assay kit	Life Technologies	Cat# Q32851
Deposited data		
Raw and analyzed scRNA seq data	This paper	GEO: GSE190839
SARS-COV-2 (Wuhan-Hu-1)	NCBI	NC_045512
SARS-CoV	NCBI	NC_004718
MERS-CoV	NCBI	NC_019843
HCoV-OC43	NCBI	NC_006213
HCoV-HKU1	NCBI	NC_006577
HCoV-NL63	NCBI	NC_005831
HCoV-229E	NCBI	NC_002645
Experimental models: Cell lines		
A549-ACE2-RFP-HLA-A*01:01	In house production	N/A
A549-ACE2-RFP-HLA-A*03:01	In house production	N/A
K562-HLA-A*01:01 BFP	In house production	N/A
K562-HLA-A*03:01 BFP	In house production	N/A
RD114	In house	N/A
Oligonucleotides		
Alt-R® CRISPR-Cas9 crRNA 5′-AGAGTC TCTCAGCTGGTACA-3′ for TRAC	IDT DNA	N/A
Alt-R® CRISPR-Cas9 crRNA 5′-GGAGA ATGACGAGTGGACCC-3′ for TRBC	IDT DNA	N/A

(*Continued on next page*)

Continued

REAGENT or RESOURCE	SOURCE	IDENTIFIER
Alt-R® CRISPR-Cas9 tracrRNA	IDT	Cat# 1072532
HDR template PCR primer fwd 5′-CTGC CTTTACTCTGCCAGAG-3′	Merck	N/A
HDR template PCR primer rev 5′- CATC ATTGACCAGAGCTCTG-3′	Merck	N/A
Recombinant DNA		
MP72 vector for retrovirus generation in RD114 cells	In house	N/A
Software and algorithms		
Affinity Designer 1.9	Serif	https://affinity.serif.com/
Cell Ranger 3.0.2/5.0.0	10X genomics	https://support.10xgenomics.com/single-cell-gene-expression/software/pipelines/latest/installation
FlowJo V10	FlowJo LLC	https://www.flowjo.com
GraphPad Prism 9	Graphpad	https://www.graphpad.com
Hla-genotyper 0.4	https://pypi.org/project/hla-genotyper/	https://pypi.org/project/hla-genotyper/
IEDB T cell epitope prediction tools	T Cell Tools	iedb.org
IncuCyte S3 Software, Version 2019B Rev2	Essen, Bioscience	N/A
Microsoft Excel	Microsoft	N/A
NETCTL1.2	NetCTL 1.2 Server	dtu.dk
NETMHC4.0	NetMHC 4.0 Server	dtu.dk
NetMHCpan4.1	NetMHCpan 4.1 Server	dtu.dk
Netstab1.0	NetMHCstab 1.0 Server	dtu.dk
PickPocket1.1	PickPocket 1.1 Server	dtu.dk
Scanpy 1.4.3	Wolf et al., 2018	https://doi.org/10.1186/s13059-017-1382-0
Scirpy 0.3	Sturm et al., 2020	https://doi.org/10.1093/bioinformatics/btaa611
scSplit 1.0	Xu et al., 2019	https://doi.org/10.1186/s13059-019-1852-7
Souporcell 2.0	Heaton et al., 2020	https://doi.org/10.1038/s41592-020-0820-1
uType software	Invitrogen/ThermoFisher	N/A
Other		
Äkta pureSuperdeso 200 10/300GL	GE	N/A
2100 Bioanalyzer	Agilent	G2939BA
3130xl Genetic Analyzer	Applied Biosystems, Darmstadt, Germany	N/A
4D-Nucleofector	Lonza	Cat# AAF-1002B AAF-1002X
Biomek NXP pipetting roboter	Beckman Coulter	N/A
CytoFlex S Cell Analyzer	Beckman Coulter	N/A
Incucyte S3 Live-Cell Analysis System	Sartorius	Cat# 4647
MoFlo Astrios EQ	Beckman Coulter	B25982
NovaSeq 6000	Illumina	N/A
SimpliAmp Thermocycler	Applied Biosystems, Darmstadt, Germany	Cat# A24811

RESOURCE AVAILABILITY

Lead contact

Further information and requests for resources and reagents should be directed to and will be fulfilled by the lead contact, Dirk H. Busch (dirk.busch@tum.de).

Materials availability

This study did not generate new unique reagents.

Data and code availability

- Single-cell RNA-seq data have been deposited at GEO and are publicly available as of the date of publication. Accession numbers (GEO: GSE190839) are listed in the key resources table. This paper analyzes existing, publicly available data. These accession numbers for the datasets are listed in the key resources table.
- This paper does not report original code.
- Any additional information required to reanalyze the data reported in this paper is available from the lead contact upon request.

EXPERIMENTAL MODEL AND SUBJECT DETAILS

Clinical samples

For symptomatic SARS-CoV-2 infections, blood sample was collected at the Helios Clinic West Munich, German Heart Center Munich and University Medicine Mannheim from healthcare employees who were diagnosed by PCR test and experienced mild symptoms (cold, cough and mild fever), for which home quarantine was sufficient (female (f)/male (m)/unknown (u), 32/19/2; age ± SD, 40.5 ± 10.6 years). Participants donated 50 ml blood at the end of the required home quarantine and repeatedly in 4, 8, 12 and 24 weeks following recovery from infection. The study cohort of asymptomatic seropositive (f/m/u, 18/10; age ± SD, 38.4 ± 13.5 years) and seronegative donors (f/m/u, 23/14; age ± SD, 38.8 ± 13.6 years) was established at the Klinikum Rechts der Isar (Munich) and included health care employees that were tested for presence of SARS-CoV-2 specific antibodies in April/May 2020. 10 ml blood was collected at two time points between August 2020 and November 2020. Frozen peripheral blood mononuclear cells (PBMCs) from pre-pandemic (unexposed) donors were received from the Institute for Transfusion Medicine Dresden and collected between 2018 and 2019 (f/m/u, 12/10; age ± SD, 42.96 ± 12.9 years) (Table S3). All participants provided informed written consent. Approval for the study design and sample collection was obtained within the framework of study "Establishment and validation of epitope-specific SARS-CoV-2 blood-based testing methods" (EPI-SARS) by the ethics committee of the Technical University of Munich (reference number 182/20) and the Institutional Ethics Committee of the University Medicine Mannheim (reference number 2020-556N).

Human primary T cells from whole blood and cell culture

PBMCs were isolated from whole blood by gradient density centrifugation according to manufacturer's instructions (Pancoll human) and frozen in fetal calf serum (FCS) + 10% DMSO for liquid nitrogen storage. For T cell analyses, PBMCs were thawed and rested for 16 h in RPMI 1640 supplemented with 10% FCS, 0.025% l-glutamine, 0.1% HEPES, 0.001% gentamycin and 0.002% streptomycin before stimulation or expansion procedures.

Virus packaging cell line RD114 and A549-ACE2 RFP^+ cell lines (with and without additional HLA class I molecules) were cultured in DMEM supplemented with 10% FCS. All cells were cultured in a humidified incubator at 37°C, 5% CO_2.

METHODS DETAILS

Detection of SARS-CoV-2 adaptive immunity

Epitope prediction

Potential $CD8^+$ T cell epitopes were predicted from all open reading frames of the Wuhan-Hu-1 reference sequence (NC_045512) for HLA Class I binding to diverse HLA molecules (HLA-A*01:01, HLA-A*02:01, HLA-A*03:01, HLA-A*11:01, HLA-A*24:02, HLA-B*07:02, HLA-B*08:01, HLA-B*35:01) using NetMHC4.0 for peptides of 8 – 11 amino acids in length. Peptide candidates with predicted binding strength < 50 nM were further evaluated for immunogenicity, TAP transport, proteasomal cleavage and processing, using the following *in silico* prediction tools: Netstab1.0, NETCTL1.2, PickPocket1.1, NetMHCpan4.1. Peptide candidates showing the highest immunogenic prediction scores were cross-referenced for sequence homology to SARS-CoV-1, MERS and common cold corona viruses HCoV-OC43 (NC_006213), HCoV-HKU1 (NC_006577), HCoV-NL63 (NC_005831) and HCoV-229E (NC_002645). Homology to common cold corona viruses was further investigated by exchanging amino acids in the epitope sequence and searching for hits in the virus genome in order to roughly access the maximum degree of homology. Peptides unique to SARS-CoV-2 with highest scores in various prediction tools were selected for further validation in an in-house peptide pool.

The peptide pool was supplemented with IEDB published SARS-CoV-2 epitopes and epitopes homologous to SARS-CoV-1 (NC_004718) and MERS (NC_019843) (Table S1).

Serology

For all time points of blood donation, a serum sample was taken and analyzed for anti-SARS-COV-2 IgG using the iFlash Immunoassay analyzer, following the manufacturer's protocol. Briefly, the serum samples were incubated with samples treatment solution and SARS-CoV-2 antigen-coated paramagnetic microparticles to form a complex. Unbound material was washed from the solid

phase and a second incubation step with Acridinium-labeled anti-human IgG conjugate followed. After washing, the pre-Trigger and Trigger solutions were added to the reaction mix and the resulting chemiluminescent reaction was measured as relative light units by the iFlash optical system. A cutoff was calculated from SARS-CoV-2 IgG calibrators.

T cell expansion with autologous peptide-pulsed PBMCs

20% of total PBMCs were pulsed with 10 μg/ml peptide pool for 2 h at room temperature under gentle agitation at $1x10^6$ cells/ml. Excess of peptides was removed by washing and peptide-pulsed cells were co-cultured with the remaining 80% of PBMCs for 10 - 12 days in RPMI 1640 supplemented with 5% human serum, 0.025% l-glutamine, 0.1% HEPES, 0.001% gentamycin and 0.002% streptomycin at $1x10^6$ cells/ml. 50 IU/ml IL-2 was added every 3 - 4 days.

Antigen-specific activation and intracellular cytokine staining

For *ex vivo* or expanded primary T cells, PBMCs were stimulated with 1 μg/ml peptide pool, 1 μg/ml peptide or 1 μg/ml PepTivator SARS-CoV-2 Protein S pool. For TCR-engineered T cells, K562 antigen presenting cells (retrovirally transduced with HLA-A1 or HLA-A3) were irradiated (80 Gy), loaded with different peptide concentrations (10^{-12}, 10^{-11} 10^{-10}, 10^{-9}, 10^{-8}, 10^{-7}, 10^{-6}, 10^{-5} and 10^{-4} M) overnight at 37°C, and co-cultured with engineered T cells in 1:1 effector:target ratio. Incubation with peptides or antigen-presenting cells was done for 4 h at 37°C, in presence of 1 μg/ml GolgiPlug. DMSO served as negative control whereas 25 ng/ml PMA and 1 μg/ml Ionomycin served as positive control. After incubation, cells were stained with EMA solution (1:1000) for live/dead discrimination and subsequently with surface antibodies: CD19-ECD (1:100), CD8-PE (1:200), CD3-BV421 (1:100) and murine TCR β-chain-APC/Fire750 (1:100). Cells were fixed using Cytofix/Cytoperm solution followed by staining for intracellular cytokine by IFN-γ-FITC antibody (1:10). Flow cytometric acquisition was performed on the CytoFlex S Cell Analyzer.

Flow cytometry cell sorting

Expanded PBMCs (day 13 post-expansion) were freshly re-stimulated with 1 μg/ml peptide for 4 h at 37°C. Peptide-reacting cells were sorted according to cytokine secretion, detected via IFN-γ catch (IFN-γ-FITC), and CD8 staining (CD8-eF450 1:200). Additionally, donor cells were stained with Total Seq-C antibodies (10x Hashtag 1-6, 0,5 mg/ml) prior sample pooling, in order to discriminate individual donors in the sequencing sample. Flow sorting of $CD8^+$ IFN-γ^+ and $CD8^+$ IFN-γ^- was conducted on a MoFlo Astrios EQ under biosafety level 3.

HLA genotyping

Generic PCR amplification of complete HLA-class I coding regions (HLA-A, -B and -C) were performed in a 11 μl polymerase chain reaction (PCR) assay using 5 μl LongAmp Taq 2x Master Mix, 3 μl forward and reverse primer mix (each 1.5 pmol/μl) and 3 μl DNA (about 10-50 ng/μl). The homemade amplification primers were located in the 5'- and 3'-untranslated region. On a SimpliAmp Thermocycler, the thermocycler profile used was a denaturation step at 94°C for 7 min, followed by 15 cycles of denaturation at 94°C for 1 min and annealing /elongation at 66°C for 5 min. Finally, 30 cycles of denaturation at 94°C for 10 s, annealing at 65°C for 50 s and elongation at 72°C for 5 min were performed, with a final hold at 20°C. If necessary, amplification control was performed loading 5 μl of the amplification product on an ethidium bromide stained agarose gel and running electrophoresis for 30 min at 180 V / 80mA.

Sanger DNA sequencing itself was run on a 3130xl Genetic Analyzer, using 5 μl Reaction Mix (composed of 0.5 μl BigDye®Terminator v3.1 Cycle Sequencing RR-100, 1.9 μl Q-solution and 2.6 μl water), 5 μl 1:20 diluted amplification product and 5 μl of homemade sequencing primer (exon 1-7; 2.5 pmol/μl). Cycle sequencing assays was performed with a 100-fold approach by a Biomek NXP pipetting roboter. Cycle sequencing itself was run in a SimpliAmp Thermocycler (94°C 2 min, 30 cycles 94°C for 10 s, 60°C 2 min, hold at 20°C). Cycle sequencing reactions were purified using Agencourt CleanSeq magnetic beads in a Biomek NXP protocol following the manufacturer's instructions. Sanger DNA sequencing itself passed on a 3130xl Genetic Analyzer. After import of sequence raw data in the uType software, the sequences were analyzed for HLA type creation by aligning to recent IMGT HLA allele database.

HLA type for asymptomatic seropositive and seronegative donors was determined via surface antibody staining using commercially available antibodies targeting HLA-A*02-FITC (1:200,), HLA-A*03-APC (1:200), HLA-B*07-PE (1:100), HLA-B*08-APCVio770 (1:200).

Single-cell RNA sequencing and data analyses

10x genomics for single-cell RNA sequencing

After sorting according to IFN-γ signal, cells were centrifuged and the supernatant was carefully removed. Cells were resuspended in the 37.2 μl Mastermix + 37.8 μl water before 70 μl of the cell suspension were transferred to the chip. (Step 1.1 and 1.2 of the original protocol). After each step, the integrity of the pellet was checked under the microscope to ensure that all cells are loaded onto the chip. From here on, 10x experiments have been performed according to the manufacturer's protocol (Chromium next GEM Single Cell VDJ V1.1, Rev D). Quality control has been performed with a High sensitivity DNA Kit on a Bioanalyzer 2100 as recommended in the protocol, and libraries were quantified with the Qubit dsDNA hs assay kit. All steps have been performed using RPT filter tips and DNA LoBind tubes.

For sequencing, libraries have been pooled according to their minimal required read counts (20.000 reads/cell for gene expression libraries and 5.000 reads/cell for TCR/surface antibody libraries). Illumina paired end sequencing was performed with 28+91 bp on a HiSeq2500 or with 2x150 bp on a NovaSeq 6000 for the second experiment. Annotation against the human genome (GRCh38) and a corresponding VDJ reference (vdj_GRCh38_alts_ensembl-3.1.0) was performed using Cell Ranger (V 3.0.2, 10x genomics) for the first experiment. For the second experiment, an updated Cell Ranger version (V 5.0.0, 10x genomics) was used in combination with updated references (GRCh38-2020-A and vdj_GRCh38_alts_ensembl-5.0.0)

Data pre-processing of single-cell RNA sequencing

Data preprocessing has been performed according to the current best practice in scRNA sequencing analysis (Lueken & Theis, https://www.embopress.org/doi/full/10.15252/msb.20188746). All analyses have been performed using SCANPY (Wolf et al., 2018). Briefly, cells with less than 200 genes as well as genes present in less than three cells were excluded. Cells with more than 20% mitochondrial genes were excluded and cut-offs for the maximum number of counts (experiment 1: 50.000, experiment 2: 40.000) and number of genes (experiment 1: 7.000, experiment 2: 6.000) were selected individually for the two experiments. Counts were normalized per cell, logarithmized and the variance was scaled to unit variance and zero mean. The number of counts, percentage of mitochondrial genes and cell cycle score was regressed out before highly variable genes were identified and filtered. The data was batch corrected using batch-balanced k nearest neighbors (bbknn) for the individual donors. Donor reallocation was performed using scSplit (Xu et al., 2019) and HLA-genotyper/gene score for Y chromosome genes (https://www.uniprot.org/docs/humchry.txt) for the first experiment, and souporcell (Heaton et al., 2020) in combination with barcoded antibodies for the second experiment. Since HLA prediction from RNA sequencing data is not very accurate, an HLA score was introduced to allocate donors to clusters derived from scSplit demultiplexing. In principle, HLA matching was scored considering all predictions and all original genotypes in order to find the best match between prediction and genotype.

Gene set definition for enrichment scoring

Genes composing the functionality signature were defined as the top genes correlating with EC_{50} values of the re-expressed TCRs (r squared > 0.5 and slope > 0.1). Genes composing the reactivity signature were defined by ranking genes per group using t-test and selecting the enriched genes of TCRs that showed an EC_{50} value after re-expression (-log10(p value) > 250). For CD8 activation score, we used the Gene-ontology CD8 activation score GO:0036037.

Clonotype definition from single-cell RNA sequencing data

Clonotype analysis was performed using scirpy (Sturm et al., 2020). Cells belonging to one clonotype were defined to have identical α and β chain CDR3 nucleotide sequences and both pairs of TRA/TRB sequences were considered in case additional chains have been present.

TCR re-expression and functional validation

TCR DNA template design and CRISPR/Cas9-mediated TCR knockin

DNA constructs for CRISPR-Cas-9-mediated homology-directed repair (HDR) at TRAC locus were designed *in silico* with the following structure: 5′ homology arm (300–400 base pairs (bp), P2A, TCR-β (including mTRBC with additional cysteine bridge (Cohen et al., 2007)), T2A, TCR-α (including mTRAC with additional cysteine bridge (Cohen et al., 2007)), bGHpA tail, 3′ homology arm (300–400 bp). All HDR DNA template sequences were synthesized by Twist and dsDNA templates were generated via PCR.

To generate 40 μM gRNAs, equal amounts of crRNA hTRAC6 (80 μM) or crRNA hTRBC3 (80 μM) were annealed with tracrRNA (80 μM) at 95°C for 5 min and let allowed to cool down to RT. 20 μM electroporation enhancer (400 μM) was added to gRNA. Cas9 (61 μM) was diluted to 6 μM or 20 μM with PBS for electroporation of $1x10^6$ cells or > $5x10^6$ cells. Final RNPs were generated by addition of equal volumes of Cas9 to gRNA and incubation for 15 min at RT. For electroporation, hTRAC6, hTRBC3 (3 μl for $1x10^6$, 1 μl for > $5x10^6$ cells) and HDR template (1 μg/$1x10^6$ cells) were incubated at RT for at least 30 sec. PBMCs isolated from whole blood of healthy donors were then resuspended in P3 buffer, added to CRISPR reagents for nucleofection (EH-100) and cultured in medium with 180 IU/ml IL-2. Antibiotics were supplemented to the media after 24 h post-nucleofection. TCR sequences for re-expression are listed in Table S4.

pHLA multimer and surface markers stainings

All pHLA monomers were produced in-house as previously described (Effenberger et al., 2019). For multimer staining, 0.4 μg biotinylated pHLA was multimerized on 0.1 μg fluorophore-conjugated StrepTavidin backbone in a final volume of 50 μl. Up to $5x10^6$ cells were incubated with 50 μl fluorescent-labelled multimers for 45 min on ice protected from light. Surface antibody staining was added after 25 min and incubated for remaining 20 min. Surface marker for TCR KI and multimer stainings covered mTRBC-PE (1:100), CD8-FITC (1:100), CD3-PC7 (1:100).

Retroviral transduction

A549-ACE2 RFP^+ cells were kindly provided by the group of Professor Andreas Pichlmair. These cells have been previously engineered to express the SARS-CoV-2 surface receptor protein ACE2 and red fluorescent protein (RFP). A549-ACE2 RFP^+ cells were then retrovirally transduced with plasmids encoding HLA-A*01:01 or HLA-A*03:01. Cells were additionally co-transduced with blue fluorescent protein (BFP) for selection of transgene expressing cells. For the production of retroviral particles, RD114 cells were transfected with pMP71 expression vector (containing the HLA heavy chain construct, gag/pol and amphotropic envelope) by calcium phosphate precipitation. For this, 15 μl of a 3.31 M $CaCl_2$ was mixed with 18 μg vector DNA and filled up to a total of 150 μl with ddH_2O. This mix was slowly added under vortexing to 150 μl transfection buffer containing 274 mM NaCl, 9.9 mM KCl, 3.5 mM Na_2HPO_4 and 41.9 mM HEPES. Subsequently, transfection mix was added to RD114 cells and incubated for 6 h at 37°C, 5% CO_2 followed by a complete medium exchange. Virus supernatant was harvested three days later and coated on retronectin-treated well plates via centrifugation at 3000 g, for 1 h at 32°C. Subsequently, $1x10^5$ A549-ACE2 RFP^+ cells were transduced via spinoculation at 2000 g for 30 min at 32°C. Successfully transduced cells were purity sorted three days after for HLA-A*03 expression. In the case of HLA-A*01, cells were sorted for BFP expression.

IncuCyte killing assay

Production and quantification of GFP-expressing SARS-CoV-2 stocks have been performed as previously described (Stukalov et al., 2021; Thi Nhu Thao et al., 2020). For the Incucyte killing assay, $5x10^3$ A549-ACE2$^+$ RFP$^+$ HLA-A*01 or A549-ACE2$^+$ RFP$^+$ HLA-A*03 cells were seeded 24 h prior infection with SARS-CoV-2 GFP virus (MOI 5). Plates were placed in the IncuCyte S3 Live-Cell Analysis System where real-time images of mock (RFP channel) and infected (GFP and RFP channel) cells were captured every 3 h for 72 h. Cell viability (mock and infected), virus growth and infected target cells were respectively assessed as the cell number per image (RFP$^+$ objects), total GFP area (μm^2) per image and overlap of object counts per image (RFP$^+$GFP$^+$ objects) using IncuCyte S3 Software (Essen Bioscience; version 2019B Rev2). SARS-CoV-2 TCR-engineered T cells were sorted on day 10 post CRISPR/Cas9 editing and were added 24 h post-infection. At endpoint (72 h post-infection), supernatant and T cells were removed, infected cells were washed once with PBS, and fresh medium was added before picture acquisition.

QUANTIFICATION AND STATISTICAL ANALYSIS

Data was displayed using GraphPad Prism (V9.1) or the seaborn (0.10.0) and matplotlib (3.1.3) packages in python. Statistical and correlation analyses were performed in GraphPad Prism and with stat.linregress method from the scipy (1.4.1) module, respectively. Significance is defined as *p-value < 0.05, **p-value < 0.01,***p-value < 0.001, ****p-value < 0.0001. Information on statistical tests used for individual figures can be found in the figure legends.